Developmental Biology 339 (2010) 338–353

Contents lists available at ScienceDirect

Developmental Biology

journal homepage: www.elsevier.com/developmentalbiology

Lack of maternal Heat Shock Factor 1 results in multiple cellular and developmental defects, including mitochondrial damage and altered redox homeostasis, and leads to reduced survival of mammalian oocytes and embryos

Christiane Bierkamp [a,*], Maëva Luxey [a], Aïcha Metchat [a,1], Christophe Audouard [a], Rémi Dumollard [b], Elisabeth Christians [a,*]

[a] Université Toulouse, UPS, UMR 5547, Centre de Biologie du Développement, IFR 109, CNRS, UPS, 118 route de Narbonne (Bat 4R3), 31062 Toulouse Cedex 09, France
[b] Laboratoire de Biologie du Développement, UMR 7009, Station Zoologique, 06230 Villefranche sur Mer, France

ARTICLE INFO

Article history:
Received for publication 28 October 2009
Revised 12 December 2009
Accepted 23 December 2009
Available online 4 January 2010

Keywords:
Oocytes
Heat shock factor
Oxidative stress
Fertilization
Survival

ABSTRACT

Heat Shock Factor 1 (HSF1) is a transcription factor whose loss of function results in the inability of *Hsf1*$^{-/-}$ females to produce viable embryos, as a consequence of early developmental arrest. We previously demonstrated that maternal HSF1 is required in oocytes to regulate expression of chaperones, in particular Hsp90α, and is essential for the progression of meiotic maturation. In the present work, we used comparative morphological and biochemical analytic approaches to better understand how *Hsf1*$^{-/-}$ oocytes undergo irreversible cell death. We found that the metaphase II arrest in mature oocytes, cortical granule exocytosis and formation of pronuclei in zygotes were all impaired in *Hsf1*$^{-/-}$ mutants. Although oogenesis generated fully grown oocytes in follicles, intra-ovarian *Hsf1*$^{-/-}$ oocytes displayed ultrastructural abnormalities and contained dysfunctional mitochondria as well as elevated oxidant load. Finally, the apoptotic effector, caspase-3, was activated in most mutant oocytes and embryos, reflecting their commitment to apoptosis. In conclusion, our study shows that early post-ovulation events are particularly sensitive to oxidant insult, which abrogates the developmental competence of HSF1-depleted oocytes. They also reveal that *Hsf1* knock-out mice constitute a genetic model that can be used to evaluate the importance of redox homeostasis in oocytes.

Introduction

Maternal effect mutations, first extensively described in flies and lower vertebrates, affect genes that encode RNAs and proteins normally stored in oocytes, which are used to support embryonic development (Schupbach and Wieschaus, 1989). In mammals, an increasing number of genes with maternal effects have been identified by gene knock-out and RNAi approaches (e.g., *Mater*, *Hsf1*, *Zar1*, *Npm2*, *CTCF* and *Basonuclin1*; reviewed in Matzuk and Lamb, 2008) and impairment of their function leads to developmental arrest before implantation. Genes with maternal effect are not all characterized by an expression exclusively restricted to the growing oocyte (e.g., *Mater*, *Zar1*). Some of them (e.g. *Hsf1*) are active in many other cell types. Moreover, maternal effect mutations may induce partial or total developmental arrest in embryos at different developmental stages, depending on the abolished function (e.g.: 1-cell (*Hsf1*), 2-cell (*Mater*)). Finally, although the processes altered in some maternal effect mutations have been identified such as zygotic genome transcription, nuclear and nucleolar organization or imprinting, the molecular roles of most maternal effect genes and their relation to embryonic development remain poorly understood (Matzuk and Lamb, 2008).

The maternal effects of Heat Shock Factor 1 (HSF1), a protein well known as the major transcriptional regulator of the heat shock response (McMillan et al., 1998, Pirkkala et al., 2001), were identified in mice a few years ago (Christians et al., 2000). The heat shock response increases the level of heat shock proteins (Hsps), which function as chaperones to counteract proteotoxic damage and promote cell survival after heat or oxidative stress (Kregel, 2002; Balch et al., 2008). The heat shock factors (HSFs) and the heat shock response are conserved from yeast through plants to animals and extensive studies have defined the highly conserved heat shock element, a specific binding site of HSF1 on its target genes (Pirkkala et al., 2001; Trinklein et al., 2004). In mammals, up to five genes coding for HSFs have been identified, mainly based on significant homology of

* Corresponding authors. Fax: +33 561 55 65 07.
E-mail addresses: bierkamp@cict.fr (C. Bierkamp), Elisabeth.Christians@cict.fr (E. Christians).
[1] Present address: European Molecular Biology Laboratory (EMBL), Meyerhofstrasse 1, D-69117 Heidelberg, Germany.

0012-1606/$ – see front matter © 2010 Elsevier Inc. All rights reserved.
doi:10.1016/j.ydbio.2009.12.037

their DNA binding domain. Three of them (*Hsf1*, *Hsf2* and *Hsf4*) have been investigated in knock-out experiments, each knock-out resulting in a different phenotype, which shows that they are unable to compensate for each other and exert specific, non-redundant functions (reviewed in Christians and Benjamin, 2006; Akerfelt et al., 2007). In particular, only *Hsf1* was found to exhibit maternal effects; it is essential for triggering the heat shock response (McMillan et al., 1998; Xiao et al., 1999; Christians et al., 2000).

Ovaries from *Hsf1*$^{-/-}$ females produce fully grown oocytes that appear normal under the microscope but are depleted in several heat shock proteins (Hsps), the most affected of which is Hsp90α. Such downregulation of Hsp90α is likely to be involved in the phenotype of partial meiotic arrest and symmetric division observed in *Hsf1*$^{-/-}$ mutant oocytes, via the deregulation of key meiotic kinases, such as CDK1 and MAPK (Metchat et al., 2009). Nevertheless, this may not fully explain the early developmental arrest at the 1–2 cell stage of embryos derived from *Hsf1*$^{-/-}$ females after natural mating, because other examples of experimental or natural mutations affecting meiosis progression (*Formin2*$^{-/-}$, LT/Sv strain) do not result in early developmental arrest (Leader et al. 2002; Dumont et al., 2007; Kaufman and Speirs, 1987). Therefore, we assumed that maternal HSF1 is required for other cellular functions and that additional, hitherto undescribed, defects result from the mutation of *Hsf1*. We were thus prompted to undertake further analytical and comparative investigations of oocytes and embryos generated by *Hsf1*$^{-/-}$ and *Hsf1*$^{+/+}$ females. We thoroughly analyzed cellular morphology, organelle ultrastructure and quantified biochemical parameters, to test the hypothesis that high levels of maternal HSF1 are required in the oocytes to maintain redox homeostasis by mediating expression of a set of Hsps, as has been reported for heart or kidney cells (Yan et al., 2002, 2005). As additional support for this hypothesis, there is evidence indicating the deleterious effects of induced oxidative stress in oocytes on mitochondrial function, Ca^{2+} homeostasis and post-fertilization development (Liu et al., 1999; Combelles et al., 2009; Dumollard et al., 2009). Our results highlight the absolute requirement of defence mechanisms orchestrated by maternal HSF1 to protect oocytes against excessive internal oxidant insult, which would otherwise disturb further development and survival.

Materials and methods

Mice

The *Hsf1* knock-out mouse line used in this study was derived from animals, that were initially created using homologous recombination with a gene targeting vector in ES-cells, described elsewhere (McMillan et al., 1998; Xiao et al., 1999). *Hsf1* knockout mice were previously provided by I.J. Benjamin (Salt Lake City, UT) and were maintained in a mixed genetic background C57BL/6J X BALB/c, generating 15% viable *Hsf1*$^{-/-}$ mice. Experimental *Hsf1*$^{-/-}$ females were produced by intercrossing *Hsf1*$^{+/-}$ females and *Hsf1*$^{-/-}$ males, both of which are fertile (Xiao et al., 1999). Wild-type (WT) *Hsf1*$^{+/+}$ age-matched females from the same mixed genetic background were obtained from intercrosses between heterozygous mice and were kept in our breeding colony along with *Hsf1*$^{-/-}$ females. Taking into account the growth retardation observed for *Hsf1*$^{-/-}$ animals (Xiao et al., 1999), we performed our experiments with females older than 2 months, which produced oocytes and responded to superovulation and mated in a similar manner as WT animals. Females were superovulated according to standard procedure (Christians et al., 1997) with an injection of 5 IU pregnant mare's serum gonadotropin (PMSG) followed 48 h later by an injection of 5 IU of human chorionic gonadotropin (hCG) and mated with WT males for the night.

Mice were genotyped at weaning and again after the experimental procedure to confirm the *Hsf1* genotype. The following two sets of primers were used to amplify i) a 560 bp fragment of exons 5 and 6 of the wild type allele (KO1: 5′CCTGTCCTGTGTGCCTAGC3′ and KO2: 5′ GTCCAACTGCCTACACAGACC3′) and ii) a 375 bp fragment of the neomycin-cassette of the mutated allele (Neo3: 5′GCCTGCTATTGTC-TTCCCAATCC3′ and Neo4: 5′ AGGACATAGCGTTGGCTACCCGTG3′).

Protocols for animal experiments were approved by the Departmental Veterinary Office (Haute-Garonne) in accordance with French legislation.

Oocyte and embryo collection and oocyte culture

Fully grown oocytes at the germinal vesicle (GV) stage were obtained by ovary puncture in a droplet of M2 medium (Sigma) containing 45 μg/ml IBMX (3-isobutyl-1-methylxanthine, Sigma) to prevent spontaneous meiosis resumption and to synchronise isolated oocytes before beginning the experiment. Following superovulation, ovulated and/or fertilized eggs were collected from ampullas and transferred in M2 medium, 24 h after hCG injection. Two-cell embryos were flushed out of oviducts at 48 h post hCG. In order to test for parthenogenetic activation of oocytes, freshly ovulated oocytes were collected from ampullas and transferred into M2 medium (Sigma) at 12 h post hCG. Groups of 10–20 oocytes were then cultured in drops of 40 μl M16 medium (Sigma) under light mineral oil (Sigma) for further 24 h in a humidified incubator maintained at 37 °C, 5% CO_2. To induce oxidant insult, GV oocytes were transferred to M16-medium containing 200 μM H_2O_2 at 37 °C for 1 h before analysis.

Immunocytochemistry of whole-mount oocytes and embryos

Oocytes and embryos were fixed with their *zonae* and processed as previously described (Christians et al., 1997; Metchat et al., 2009; Liu et al., 2005). We used several dyes: (1) the Oregon green 488 phalloidin (emission at 488 nm) and Alexa Fluor-546 phalloidin (emission at 546 nm) (Molecular Probes, 1:40 dilution at 5 U/ml) to stain actin filaments; (2) the *Lens culinaris* agglutinin fluorescein isothiocyanate (LCA-FITC) (Sigma, 100 μg/ml) to stain cortical granules. Immunodetection was performed with the following primary antibodies: (1) the rabbit anti-Histone H3 dimethyl K9 antibody (Upstate, 1:500) to stain the maternal pronucleus; (2) the rabbit anti-beta-COP antibody (Affinity Bioreagents, 1:400) to stain the Golgi complex. The following secondary antibodies were used: the goat anti-rabbit-alexa-546 antibody (Molecular probes, 1:1000; emission at 546 nm). After staining, the cells were mounted in Mowiol (Fluka) containing either PI (propidium iodide, BD Pharmingen, 1:10) or DAPI (4′,6-diamidino-2-phenylindole, Sigma, 2 μg/ml), to counterstain either chromosomes or nuclei.

Image acquisition and numerical treatment

Oocytes and embryos were analyzed under either a confocal laser microscope (CLSM Leica TCS2, (Plateforme Toulouse RIO-Imaging, CBD-IFR109) coupled to a CCD camera and treated with Leica Confocal Software (LCS), or a wide-field inverted Leica DMIRBE 2 (imaging facilities—Toulouse RIO-imaging, IEFG-IFR109). All figures were initially assembled with Adobe Photoshop software.

Transmission electron microscopy

Electron microscopical analysis was performed on ovaries from mice older than 2 months, as previously described (Carabatsos et al., 1998). Briefly, ovaries were fixed in 2% glutaraldehyde, 3% paraformaldehyde in 0.1 M cacodylate buffer, pH 7.4, followed by 1% osmium tetroxide. Specimens were rinsed in water and treated *en bloc* with 0.5% uranyl acetate. Specimens were further dehydrated in graded alcohol/propylene oxide solutions, followed by propylene

oxide/epoxy resin infiltration and embedded in epoxy resin. Ultrathin sections of 70 nm thickness were cut on an Ultracut Leica ultratome. The sections were placed on copper grids, stained with uranyl acetate and lead citrate and examined in a Jeol 100 CX transmission electron microscope coupled to a digital camera AMT (imaging facilities—Toulouse RIO-imaging, IEFG-IFR109). Four ovaries, corresponding to different females were evaluated per genotype. On sections of each ovary, the surface of several oocytes was subdivided into different areas of 20 μm^2 surface. Each area was imaged and subsequently analyzed for (a) the total number of mitochondria, (b) the number of normal mitochondria based on the morphological criteria mentioned in the results section (Wassarman and Josefowicz, 1978; Perez et al., 2007) and (c) the number of abnormal mitochondria based on the criteria explained in the results section. The percentage of abnormal mitochondria of all mitochondria was calculated for each area. More than 5 areas per oocyte were analyzed (=1 experimental group). In total, 8 oocytes from 4 control ovaries (each ovary corresponding to a different female, $N=4$ control females) and 10 oocytes from 4 different *Hsf1*$^{-/-}$ ovaries (each ovary corresponding to a different female, $N=4$ *Hsf1*$^{-/-}$ females) were analyzed. The percentages of abnormal mitochondria per area were averaged for all areas of a given genotype and the mean ± SEM expressed in the graph.

Quantification of cortical granules

GV oocytes and 1-cell embryos, collected from WT and mutant females, were stained for F-actin (phalloidin) and cortical granules (LCA-FITC) and analyzed by confocal microscopy. On single confocal sections, oocyte cortex was subdivided into areas of 50 μm^2 surface along the oocyte circumference. For each area, the LCA-positive cortical granules (CG) were counted and the mean value per oocyte was calculated. The mean number of cortical granules at the GV stage (before exocytosis) of a given genotype was normalized to 100% and the numbers of cortical granules at 1-cell embryos (after exocytosis) were expressed as percentages of that measured at the GV stage. Two females and at least 15 oocytes or 1-cell zygotes of each genotype were analyzed.

Quantification of beta-COP staining

Confocal laser scanning acquisitions were imported and analyzed using ImageJ64 software to generate a surface plot in the form of a 3D graph of the beta-COP signal intensities for WT and mutant GV oocytes. Background staining was measured and subtracted. Six to 10 particles per GV oocyte and 19–30 oocytes per genotype (corresponding to 3 females per genotype) were analyzed and their relative fluorescence intensity was calculated after subtraction of the background. The values for *Hsf1*$^{-/-}$ were calculated with respect to those of WT, normalized to 100%.

Analysis of reactive oxygen species (ROS) content

ROS level was determined with the fluorescent probe, 2′,7′-dichlorodihydrofluorescein diacetate (H2DCFDA; Sigma), as previously described (Perez et al., 2007). GV oocytes were incubated for 15 min in a freshly prepared KSOM medium containing 1 μM H2DCFDA at 37 °C. After extensive washing in fresh KSOM/HEPES, oocytes were imaged using an inverted fluorescence microscope with an FITC filter. Control oocytes (unstained) were incubated with an appropriate volume of vehicle (DMSO/KSOM) before imaging. For a positive control of oxidative stress, WT GV oocytes were cultured with M16 medium containing 200 μM H_2O_2 (Sigma) for 1 h to induce oxidant insult before being imaged for ROS content. In 4 experiments, 40 WT oocytes and 39 *Hsf1*$^{-/-}$ oocytes collected from a total of 4 females per genotype were examined.

Measurements of oxidized mitochondrial flavoprotein (FAD^{++}) autofluorescence

Measurements were carried out on WT and *Hsf1*$^{-/-}$ metaphase II oocytes as previously described (Dumollard et al., 2004). Oxidised flavoprotein (FAD^{++}) autofluorescence was analyzed using inverted fluorescence microscopy ($\lambda_{ex}=440$–490 nm, $\lambda_{em}=520$ nm). Measurements of FAD^{++} autofluorescence were obtained from the entire oocyte area and averaged for each oocyte. Arbitrary units of FAD^{++} fluorescence intensity were presented as a mean value calculated from 6 independent experiments, with 4–8 oocytes per genotype and experiment ($N=4$ females per genotype), so 28 WT oocytes and 32 *Hsf1*$^{-/-}$ oocytes were analyzed in total.

Caspase-3 assay for detection of apoptosis

Activated caspase-3 was detected in GV oocytes and 1-cell embryos using the PhiPhilux G1D2 kit (OncoImmunin Inc., College Park, MD) according to the manufacturer's protocol, with slight modifications (Kawamura et al., 2003). Briefly, 10–15 GV oocytes and 1-cell embryos were washed three times in M16 medium and incubated with 30 μl caspase-3 substrate for 1 h at 37 °C in 5% CO_2. After three washes in dilution buffer, embryos were fixed with 1% paraformaldehyde (PFA) in PBS containing 0.1 mg/ml polyvinylalcohol for 30 min at 4 °C in the dark. After three washes in PBS, embryos were transferred on to a slide containing Mowiol and analyzed under a fluorescence microscope.

Statistical analysis

For each experiment, oocytes and embryos obtained from one female were counted and/or analyzed. The corresponding numbers or measured values were compiled in Microsoft Excel spreadsheet and further analyses of the data such as proportions, percentages and mean values were calculated. Mean values between groups were compared using Student *t*-test. Differences between means were considered biologically significant at a *p*-value of less than 0.05. Data are presented as the mean ± SEM.

Results

Post-ovulation developmental events are altered in mutated oocytes

Fertilization of ovulated oocytes arrested in metaphase II induces several cellular events such as meiosis achievement, extrusion of the second polar body and formation of the two maternal and paternal pronuclei. These constitute useful criteria to determine whether development has been successfully initiated. In order to analyze the appearance of abnormal developmental events in embryos produced by *Hsf1*$^{-/-}$ females, we examined and compared the intracellular morphology of large cohorts of 1-cell embryos collected from superovulated *Hsf1*$^{+/+}$ (WT) and *Hsf1*$^{-/-}$ (mutant) females mated with WT males. We expected to see one or two polar bodies (PB) and two pronuclei (PN) in zygotes or 1-cell embryos (Figs. 1A–C). To distinguish maternal and paternal pronuclei, we used an anti-H3K9me2 antibody, which recognizes histone H3 with methylated lysine, only present in maternal chromatin (Liu et al., 2004; Figs. 1D–F). We considered ovulated oocytes as unfertilized when there was no pronuclear structure or sperm head (SH) (Fig. 1C).

First, we found that the proportion of zygotes with two PNs was significantly reduced ($p=0.0009$) in *Hsf1*$^{-/-}$ females (24%) compared to *Hsf1*$^{+/+}$ animals (75%) (Figs. 1A, D, E, G, see Table S1); most mutant oocytes contained a single PN (47% in the case *Hsf1*$^{-/-}$ females, whereas only 5% were seen in WT females; Figs. 1B, F, G, Table S1). This could be due to spontaneous (parthenogenetic) activation of oocytes, a process that releases metaphase II arrest,

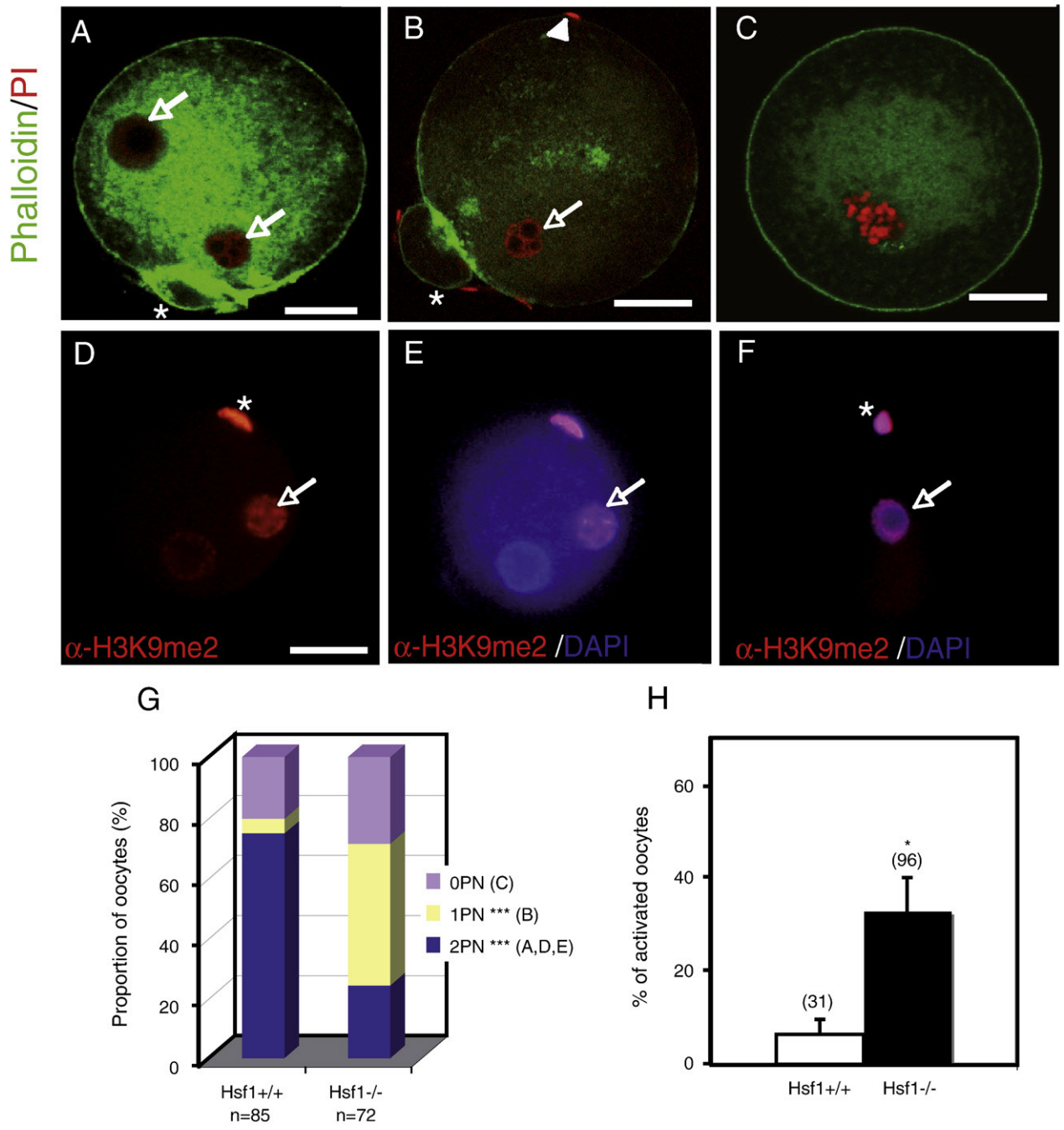

Fig. 1. Morphology of 1-cell embryos collected from *Hsf1*$^{-/-}$ females 24 h after hCG and mating. (A–C) Zygotes were stained with phalloidin (actin, green) and PI (DNA, red) and analyzed by confocal miscroscopy. (A) Normal zygote with 2 pronuclei (2PN, arrows) and one polar body (PB) (asterisk). (B) Abnormal oocyte with one PB (asterisk) and a single pronucleus (1PN) (arrow) and a sperm head (SH, arrowhead). (C) Unfertilized oocyte with one chromosomal mass. (D–F) 1-cell embryos were stained with α-H3K9me2 to label the maternal pronucleus (D, α-H3K9me2, red) and combined with DAPI (E, F, DNA, blue and α-H3K9me2, red). Asterisk indicates the PB. Scale bars: (A–C) 20 μm; (D–F) 30 μm. Note both, maternal and paternal pronuclei in the zygote in (D, E), whereas one maternal but no paternal pronucleus is detected the 1-cell embryo in (F) (Parthenote). (G) Quantification of the different phenotypes of 1-cell embryos collected from WT females ($N=5$ females) and *Hsf1*$^{-/-}$ females ($N=4$ females). Results are presented as mean percentage calculated from 4-5 independent experiments. Observed distribution for each phenotype in mutant group was compared with wild-type group, error bars correspond to SEM (Table S1; $p<0.001$). (H) Percentage of spontaneously activated (parthenogenetic) oocytes collected directly after ovulation (12 h post hCG) from WT and *Hsf1*$^{-/-}$ females and cultured in vitro for 24 h before analysis. Results are presented as mean percentage calculated from at least 3 independent experiments and error bars correspond to SEM (Table S2; $p<0.05$).

induces cortical granules exocytosis, inhibits sperm penetration and allows maternal chromatin to decondense and often form only one PN. To further determine whether *Hsf1*$^{-/-}$ oocytes displayed increased parthenogenetic activation, we dissected freshly ovulated oocytes at 12 h post hCG and cultured them *in vitro* for 24 h before observation. Significantly more ($p=0.0002$) mutant (33%) than WT (6%) oocytes contained a PB and a single pronucleus, (Fig. 1H, Table S2), confirming that *Hsf1*$^{-/-}$ oocytes were prone to parthenogenesis.

Second, we noted that in a large proportion of oocytes, a higher density of sperm heads (>1 SHs) was located in the perivitelline space of mutant than WT oocytes and zygotes. Confocal microscopy analysis and three-dimensional reconstruction revealed that most often (75%)

these extra sperm heads were attached to the plasma membrane, or penetrating it and, occasionally, (25%) decondensing in the cytoplasm (Figs. 2A–C). Since similar observations were made with non-superovulated females (data not shown), we concluded that the anomalies described above were not directly linked to hormonal treatment.

We next asked whether the presence of "extra sperm heads" in mutant oocytes depended on whether or not they were spontaneously activated. We re-analyzed the data and found that the majority of mutant oocytes with extra sperm heads had only 1PN (61%, Fig. 2D), indicating that, in the absence of maternal HSF1, enhanced spontaneous activation was phenotypically associated with massive attachment of supernumary sperm heads. In mice, the zona pellucida usually blocks the entry of further sperm after activation and cortical granule exocytosis, which biochemically modifies zona pellucida

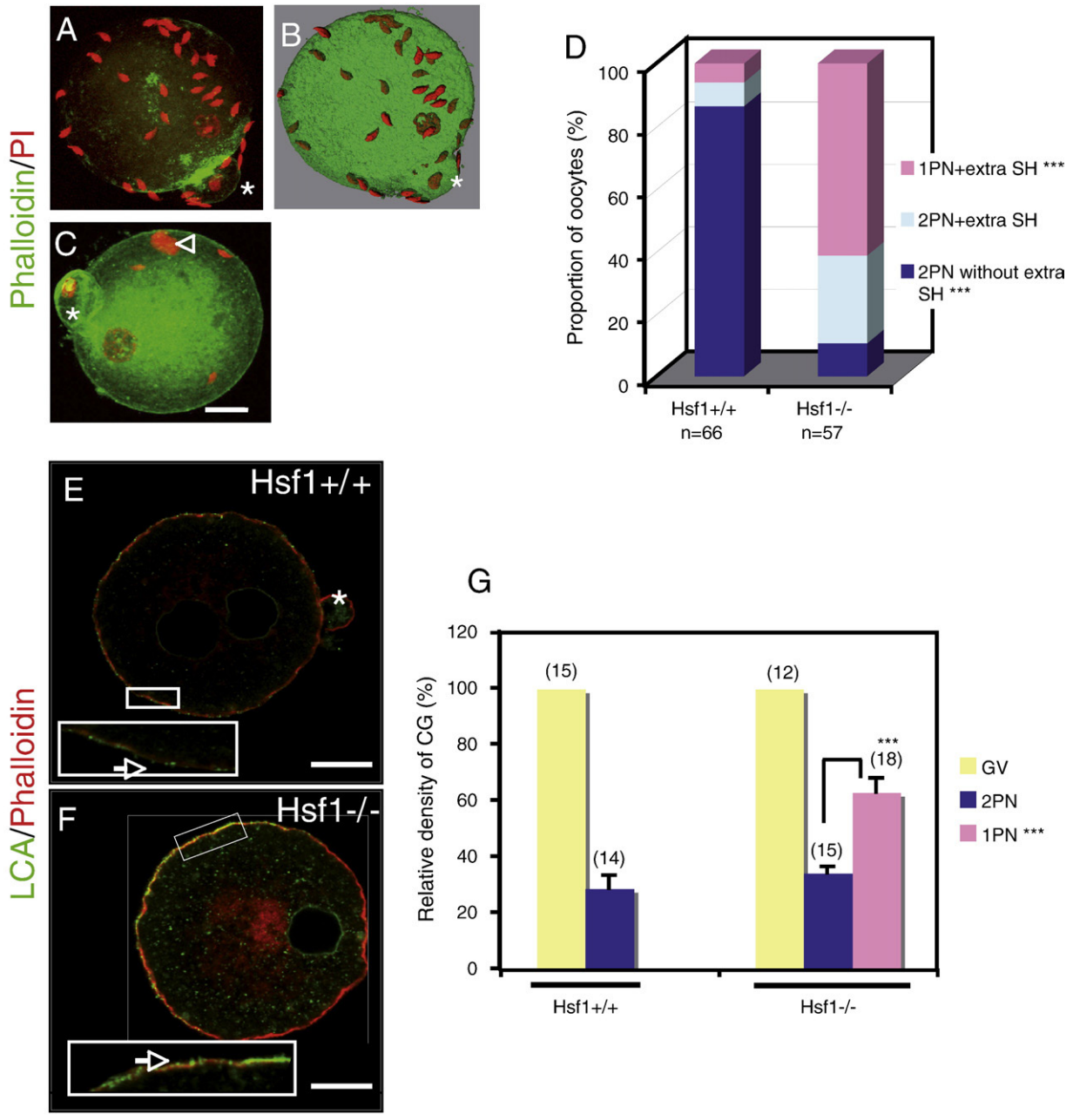

Fig. 2. Extra sperm heads (SH) binding to 1-cell embryos from *Hsf1*$^{-/-}$ females (24 h post hCG) and analysis of cortical granules exocytosis. (A–B) Images of a mutant 1-cell embryo stained with phalloidin (actin, green) and PI (DNA, red). (A) Spontaneously activated mutant 1-cell embryo with a PB (asterisk) and one PN, presenting numerous bound extra SHs. (B) Three dimensional reconstruction of embryo shown in (A), with polar body (asterisk), internal sperm heads (colored in brown) and attached sperm heads (colored in red). (C) Spontaneously activated mutant 1-cell embryo, with PB (asterisk) and one PN, in addition to some extra bound SHs, one of them decondensing in the cytoplasm (arrowhead). (D) Quantification of WT ($N=5$ females) and mutant ($N=4$ females) 1-cell embryos showing presence of extra binding SH, penetrating the plasma membrane or decondensing in the cytoplasm. Results are presented as mean percentage. Observed distribution for each phenotype in the mutant group was compared with the wild-type group (Table S3; $p<0.001$). (E–F) 1-cell embryos (24 h post hCG) stained with LCA-FITC (cortical granules, green) and conjugated phalloidin (F-actin, red). (E) WT 1-cell embryo exhibiting weak LCA-staining after cortical granules exocytosis (arrow) (see inset for higher magnification of the cortex). (F) Mutant 1-cell embryo with stronger LCA-staining due to abundant cortical granules remaining in the cortex (arrow). Scale bars: (A–C, E, F) 20 μm. (G) Quantification of FITC-LCA-labelled cortical granules localized in the cortex of WT ($N=2$ females) and mutant ($N=3$ females) GV stages (before CG exocytosis), zygotes (2PN; after CG exocytosis) and spontaneously activated, fertilized 1-cell embryos (1PN; reduced exocytosis). Results are presented as mean percentage calculated from 3 independent experiments and error bars correspond to SEM (Table S4; $p<0.001$).

glycoproteins (Sun, 2003; Ducibella, 1996; Liu et al., 2005). Thus, this first block to polyspermy appeared to be deficient in mutant oocytes. We examined the zona pellucida regarding its thickness, ultrastructural morphology and the presence of zona pellucida proteins 1,2,3, but no difference could be detected between the zona pellucida of mutant and wild type oocytes (data not shown). Then we analyzed the relative density of cortical granules as a marker of distribution and abundance of cortical granules in mutant and WT oocytes and eggs stained with fluorescein isothiocyanate-labelled *Lens culinaris* agglutinin (FITC-LCA) (Liu et al., 2005) (Figs. 2E–G). There was no difference between pre-ovulatory mutant and WT oocytes collected at the GV stage. After fertilization, only very few of the mutant zygotes (11%) in contrast to most WT zygotes (86%) contained 2PN (11%) and had a low relative density of cortical granules (34%), reflecting that this small group of mutant zygotes was capable of normal exocytosis (Figs. 2E, G). In contrast, most mutant (fertilized) oocytes with sperm heads and 1PN (61%) had a significant higher relative density of granules (63%, Figs. 2F, G). Thus, while a large proportion of *Hsf1*$^{-/-}$ oocytes seem to be spontaneously activated, this activation is associated with a reduced extent of cortical granules exocytosis.

Embryos from Hsf1$^{-/-}$ *females degenerate before the 2-cell stage*

Females from several experimental or spontaneously mutated mouse lines (e.g., *Mos* knock-out, LT/Sv strain) produce oocytes whose meiotic progression is disturbed and that are frequently parthenogenetically activated. These activated oocytes are able to pursue their development beyond the 1- to 2-cell stage (Kaufman and Speirs, 1987; Colledge et al., 1994; Hashimoto et al., 1994). In contrast, we had previously reported that the *Hsf1* mutation seemed to block any kind of development as early as the 1- to 2-cell stage (Christians et al., 2000). Therefore, we decided to re-examine carefully the developmental

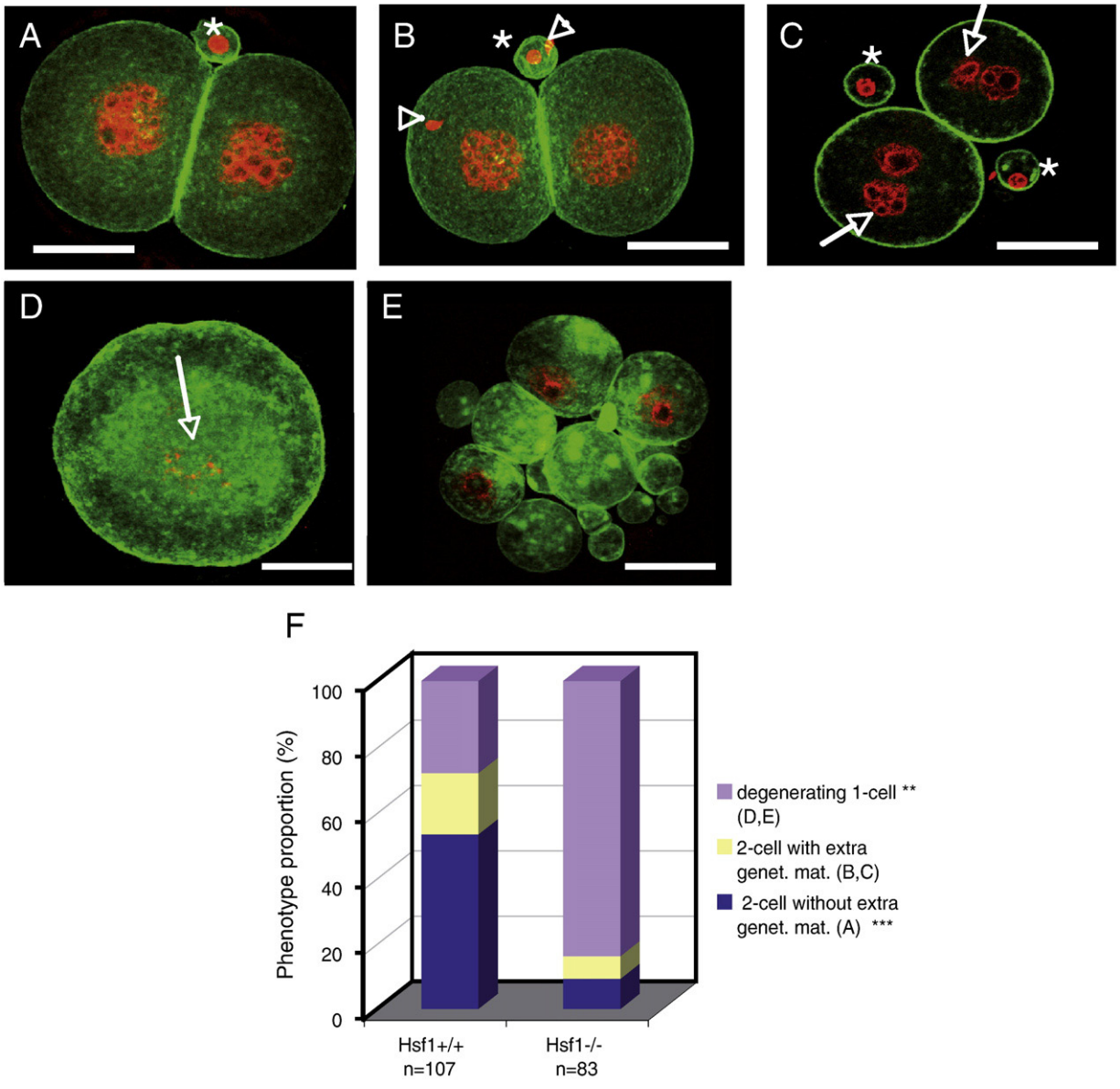

Fig. 3. Morphology of 2-cell embryos collected from *Hsf1*$^{-/-}$ females 48 h post hCG and stained with conjugated phalloidin (actin, green) and PI (DNA, red). (A) Normal 2-cell embryo. Note the presence of a PB (asterisk). (B) 2-cell embryo with two additional SHs; (arrowheads). (C) 2-cell embryo with 2 nucleus-like structures (arrows) per cell and additional SHs in the perivitelline space. (D) Degenerating embryo showing DNA fragmentation (arrow). (E) Fragmented embryo displaying membrane blebbing and many F-actin aggregates. Scale bars: (A–E) 30 μm; (F) Quantification of the different morphologies of the embryos: degenerating 1-cell embryos and 2-cell embryos with or without extra genetic material. Results were compared between WT females ($N=6$ females) and *Hsf1*$^{-/-}$ females ($N=7$ females) and are presented as mean percentage calculated from 7 independent experiments. Observed distribution for each phenotype in mutant group was compared with WT group (Table S5; $p<0.001$).

potential of fertilized mutant oocytes with either 1 or 2 PN. We collected and examined embryos from mutant and WT females at 48 h post hCG, well after the first cleavage is expected to occur (between 31 to 36 h post hCG) (Figs. 3A–E). Provided that all zygotes and activated oocytes divided normally, we should have observed 2-cell embryos, with or without extra SHs, at predictable frequencies (compare with Fig. 1F). In contrast to WT, the vast majority of embryos obtained from *Hsf1*$^{-/-}$ females (84%) appeared degenerated, displaying DNA and/or cytoplasmic fragmentation (Figs. 3D–F). This largely exceeded the population of incompetent unfertilized oocytes (29%) that we had identified in the previous experiment carried out at 24 h post hCG. Finally, only markedly few mutant 2-cell embryos were detected, at a much lower frequency than expected, and these were apparently unable to undergo further development, as we never observed later stages (Figs. 3B, F and data not shown).

Mitochondria exhibit ultrastructural and functional defects associated with increased oxidant load in mutant oocytes

In order to explain this early developmental arrest in HSF1-deficient oocytes, defects additional to those responsible for spontaneous activation and inefficient polyspermy block were likely to be implicated. We suspected defects that could potentially concern the quality of the cytoplasm, organelles, cytoskeleton or the cortex of the mutant oocyte.

We first examined mitochondria, since they represent important and abundant organelles in oocytes. Using electron microscopy, we observed that WT and mutant oocytes at the GV stage did not present obvious differences concerning size and number of mitochondria (data not shown), which were located in small clusters and often made contacts with the endoplasmic reticulum (Fig. 4). In WT oocytes, mitochondria had the characteristic round or oval shape as well as particular features of inner membrane invaginations (cristae) and matrix structure described elsewhere for fully grown oocytes. These included a large central vacuolated crista and additional cristae located in the periphery of the mitochondrion (Wassarman and Josefowicz, 1978; Perez et al., 2007). However, mitochondria in mutant oocytes appeared abnormal: there was no central crista, which was replaced by an electron dense matrix, and the peripheral cristae were columnar rather than peripherally organized or often transformed into vesicle-like structures (Figs. 4C–E). As cristae are the sites where respiration occurs, cristae organization is supposed to be

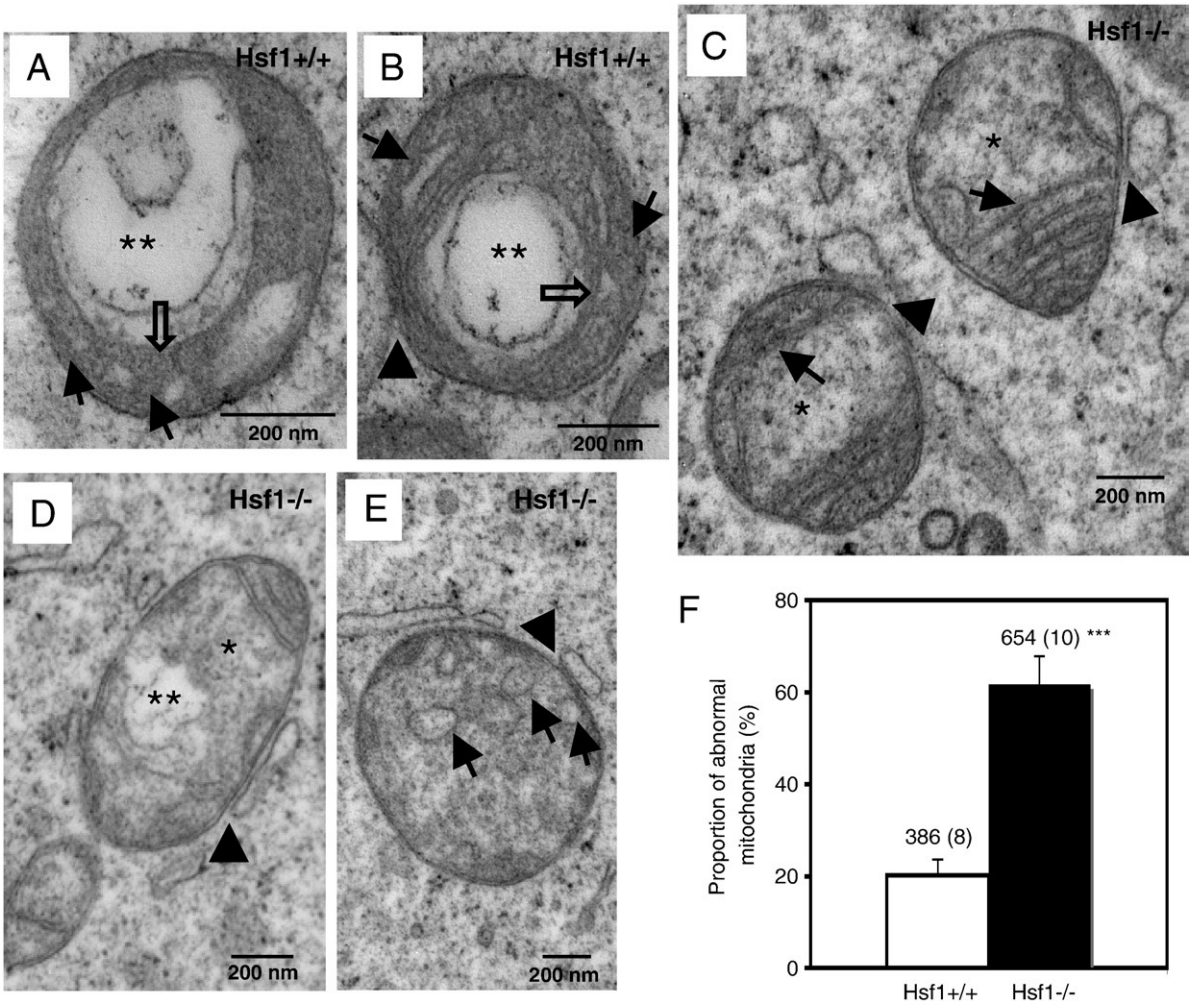

Fig. 4. Mitochondria of *Hsf1*$^{-/-}$ pre-ovulatory (GV) oocytes analyzed by electron microscopy. (A–B) Ultrastructural morphology of mitochondria from WT oocytes. (A, B) Round-oval mitochondria with a large, central vacuolated (double asterisks) cristal compartment (empty arrow) and serial lamellar cristae located in the periphery (arrows), as described elsewhere (Perez et al., 2007; Wassarman and Josefowicz, 1978). (C–E) Mitochondria from oocytes derived from *Hsf1*$^{-/-}$ females. (C) Round-oval mitochondria showing absence of the large single central vacuolated cristal structure, which is replaced by an amorphous matrix (asterisk). Additionally, lamellar cristae are no longer organized in the periphery but are arranged transversally (arrow). (D) Another example of mitochondria from an *Hsf1*$^{-/-}$ oocyte with a vacuole (double-asterisk), as well as a considerably altered central crista, that is already replaced by matrix (asterisk). (E) Additional example of mitochondria from an *Hsf1*$^{-/-}$ oocyte, where lamellar cristal structures seem to have been transformed into vesicular structures (arrows). Note the contacts between WT or mutant mitochondria with vesicles resembling the endoplasmic reticulum in (B–E) (arrowheads). Scale bars represent 200 nm. (F) Quantification of abnormal mitochondria (such as (C) and (E)) after analysis of 386 mitochondria in 8 WT oocytes ($N=4$ females) and 654 mitochondria in 10 mutant oocytes ($N=4$ females). Results are presented as mean percentage and error bars correspond to SEM (Table S6; $p<0.001$).

essential for mitochondrial function and abnormal architecture possibly be associated with dysfunction. Since it was possible that organelle orientation might have resulted in some morphological differences between single wild type and mutant mitochondria, we decided to quantify a large number of mitochondria in oocytes from several wild type (386 mitochondria) and mutant females (654 mitochondria). Quantification of abnormal mitochondria confirmed a significantly higher ($p = 0.0002$) proportion of these mitochondrial dimorphisms in mutant oocytes (62%) (Fig. 4F).

Because such abnormal degenerative features could reflect abnormal function and possible changes in redox balance (Perez et al., 2007; Ramalho-Santos et al., 2009), we measured the levels of cellular reactive oxygen species (ROS) and oxidized mitochondrial flavoproteins (FAD^{++}). To determine the levels of ROS we used the ROS indicator H2DCFDA. Among freshly isolated oocytes (GV), mutant oocytes displayed significantly higher ($p = 0.02$) levels of ROS than WT oocytes, similar to those of WT oocytes after oxidant insult (Figs. 5A, B). When freshly ovulated metaphase II oocytes from mutant and WT females were analyzed for autofluorescence of FAD^{++}, mutant oocytes had significantly higher ($p = 0.02$) arbitrary units of fluorescence intensity of oxidized FAD^{++} (245 units) compared to WT oocytes (165 units) (Figs. 5C, D), indicating that mitochondria were

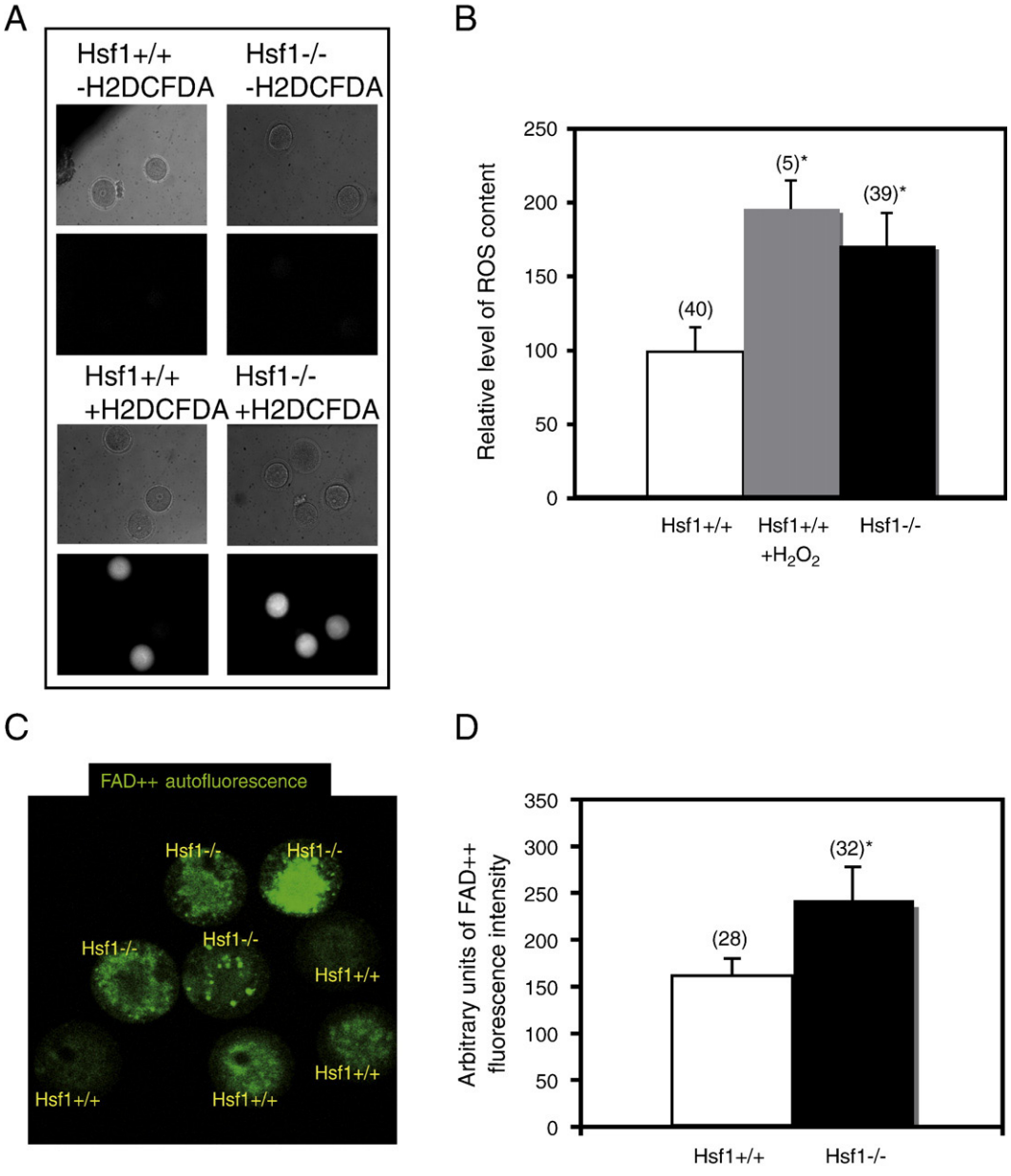

Fig. 5. Effect of absence of maternal HSF1 on cellular levels of reactive oxygen species (ROS) and on mitochondrial function in oocytes. (A) WT (left panels) and $Hsf1^{-/-}$ (right panels). GV oocytes were dissected and incubated without (upper panel) or with (lower panel) the ROS-sensitive fluorescent dye H2DCFDA. Note the two bright oocytes and one moderately fluorescing $Hsf1^{-/-}$ oocyte in the lower right panel. (B) Quantification of relative ROS levels in oocytes based on H2DCFDA-mediated fluorescence. Levels were quantified for WT oocytes, WT oocytes after oxidant insult, as a positive control for increased ROS levels (oocytes were incubated in medium + 200 μM H_2O_2 for 1 h, before analysis) and $Hsf1^{-/-}$ oocytes. Results are presented as mean percentage calculated from 4 independent experiments (except in the case of WT oocytes after oxidant insult, which were analyzed in 1 experiment), and error bars represent SEM. (Table S9; $p<0.05$). (C) Imaging of mitochondrial oxidized flavoproteins (FAD^{++}) autofluorescence (green) in $Hsf1^{+/+}$ and $Hsf1^{-/-}$ metaphase II oocytes . Note the bright $Hsf1^{-/-}$ oocyte in the upper right corner. (D) Quantification of arbitrary units of FAD^{++} fluorescence intensity in WT and $Hsf1^{-/-}$ metaphase II oocytes, based on FAD^{++} autofluorescence measured in the entire area of an oocyte and meaned for each oocyte. Results are presented as mean value calculated from 6 independent experiments, with 4-8 oocytes per genotype and experiment ($N = 4$ females per genotype) and error bars correspond to SEM (Table S9; $p<0.05$).

strongly oxidized (Dumollard et al., 2004). These observations confirmed that mutant oocytes have increased oxidant load and abnormal mitochondria with signs of oxidative damage.

Multiple cellular structures are severely affected in mutant oocytes

In addition to abnormal mitochondria, we found several other degenerative features in mutant pre-ovulatory oocytes. First, the Golgi apparatus was no longer organized in the form of cisternal stacks around the GV, as it is in WT oocytes (Figs. 6A–B), but was rather disrupted into small vesicular structures (Figs. 6C–E). We stained the Golgi stacks with antibodies against the well-known Golgi-marker beta-COP and we observed a significant loss of stacks with redistribution of beta-COP into the cytoplasm of mutant oocytes. This confirmed the disruption of the Golgi apparatus (Figs. 7A–E). Second, we noticed that the cortical actin cytoskeleton stained with conjugated phalloidin was less dense and rather disorganized in mutant oocytes (Figs. 8A–D). This finding was confirmed by electron microscopy, which revealed discontinuous, interrupted filaments beneath the plasma membrane of mutant oocytes (Figs. 8E–G). Third, cytoplasmic aggregates were more frequently identified in mutant than in WT oocytes. Many of those aggregates were positive for FITC-conjugated *Lens culinaris* agglutinin (LCA), which labels the content of trafficking vesicles (Figs. 9A, C, D), while other aggregates reacted with conjugated phalloidin, which stains actin filaments (Figs. 9B, C, E). Thus HSF1-deficient oocytes also accumulate abnormal maternal products.

Induced apoptotic cascade in mutant oocytes and 1-cell embryos

The numerous defects found in mutant oocytes, in addition to the increased cell fragmentation (Fig. 3E), suggested that the apoptotic cascade had been activated. We addressed this question by evaluating the level of fluorescence produced by the caspase-3 substrate PhiPhiLux G1D2 and we indeed observed activated caspase-3 significantly more often in mutant than in WT oocytes or 1-cell embryos, which also included a limited proportion (<10% data not shown) of degenerated oocytes/zygotes independent of the genotype. Furthermore, the level of caspase-3 activity was also higher in mutant oocytes and similar to that in WT oocytes subject to an experimentally applied oxidant insult (Figs. 10A–H). These data demonstrate that mutant oocytes, even though they did not seem to degenerate by massive atresia within the ovary (data not shown), were committed to cell death after ovulation.

Discussion

Our original description of the *Hsf1* maternal effect mutation indicated that embryos from HSF1-deficient mothers were arrested at the 1–2 cell stage, irrespective of their own *Hsf1* genotype (Christians et al., 2000). As most maternal effect mutations described so far in mammals block embryo development at later stages, this remained a unique and intriguing developmental phenotype that is not yet fully understood. Interactions between the somatic follicular cells and the oocyte play a complex and important role for oocyte developmental competence (Eppig et al., 2000), rising the possibility of a maternal role for HSF1 in the somatic cells of the follicle. Since HSF1 expression is not restricted to oocytes, but considerably more abundant in the oocyte than in the surrounding follicular cells (Metchat et al., 2009), a maternal role for HSF1 in somatic, follicular cells seems rather unlikely. Nevertheless, to address this question further, studies based on chimeric reaggregated ovaries (Eppig et al., 2000) or on tissue-specific knock-outs of *Hsf1* in the germline versus in the somatic cell line would be particularly useful. In the present study, we first show that the *in vivo* production of normal zygotes by *Hsf1*$^{-/-}$ females is

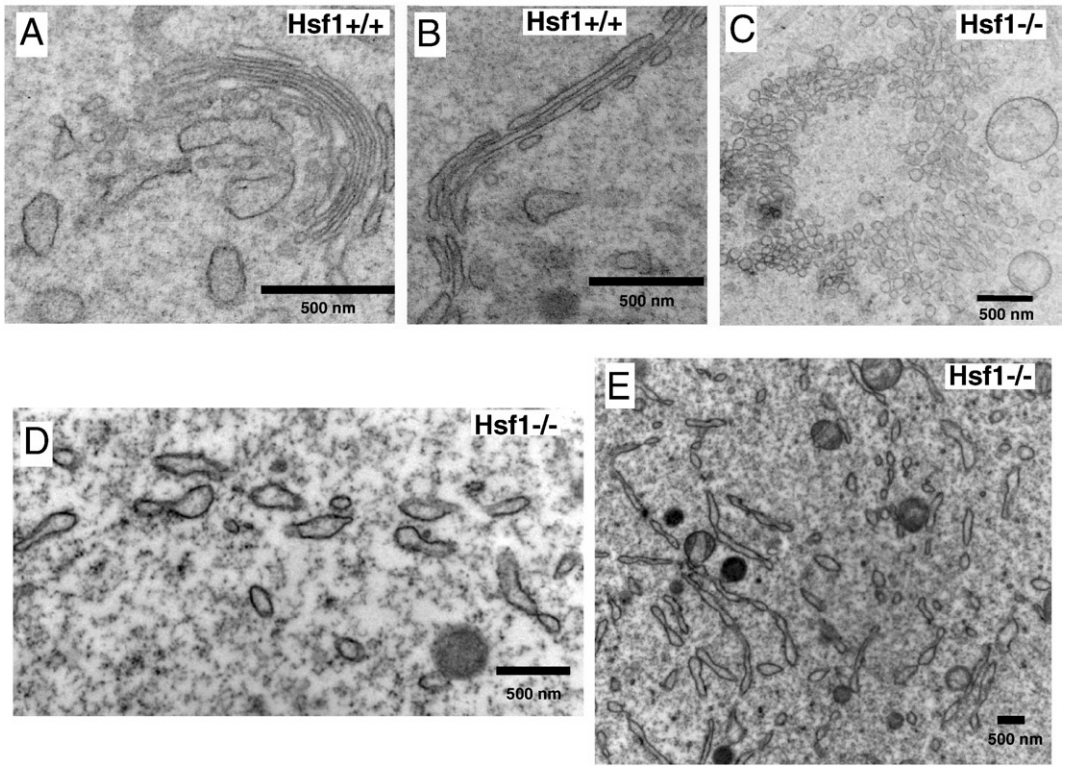

Fig. 6. Electron microscopical analysis of Golgi apparatus of *Hsf1*$^{-/-}$ pre-ovulatory (GV) oocytes (ovaries). (A, B) The Golgi compartment in WT oocytes appears as described elsewhere (Wassarman and Josefowicz, 1978), in form of long stacked, connected cisternal compartments organized semicircular (A) or stretched (B) through the ooplasm. Vesicles and vacuoles are found in proximity, suggesting trafficking activity. (C–E) The Golgi compartment in *Hsf1*$^{-/-}$ oocytes seems no longer to be organized in cisternae, but rather fragmented into many diffusing elongated vesicular structures. (C) Many of these vesicle-like structures are grouped together. (D) Elongated vesicular structures randomly diffusing through the ooplasm. (E) Low magnification overview of a zone rich in randomly dispersed elongated Golgi-like structures. (A–E) Images represent results obtained from independent observations of 8 oocytes from 4 WT females and at least 10 oocytes from 4 *Hsf1*$^{-/-}$ females. Scale bars represent 500 nm.

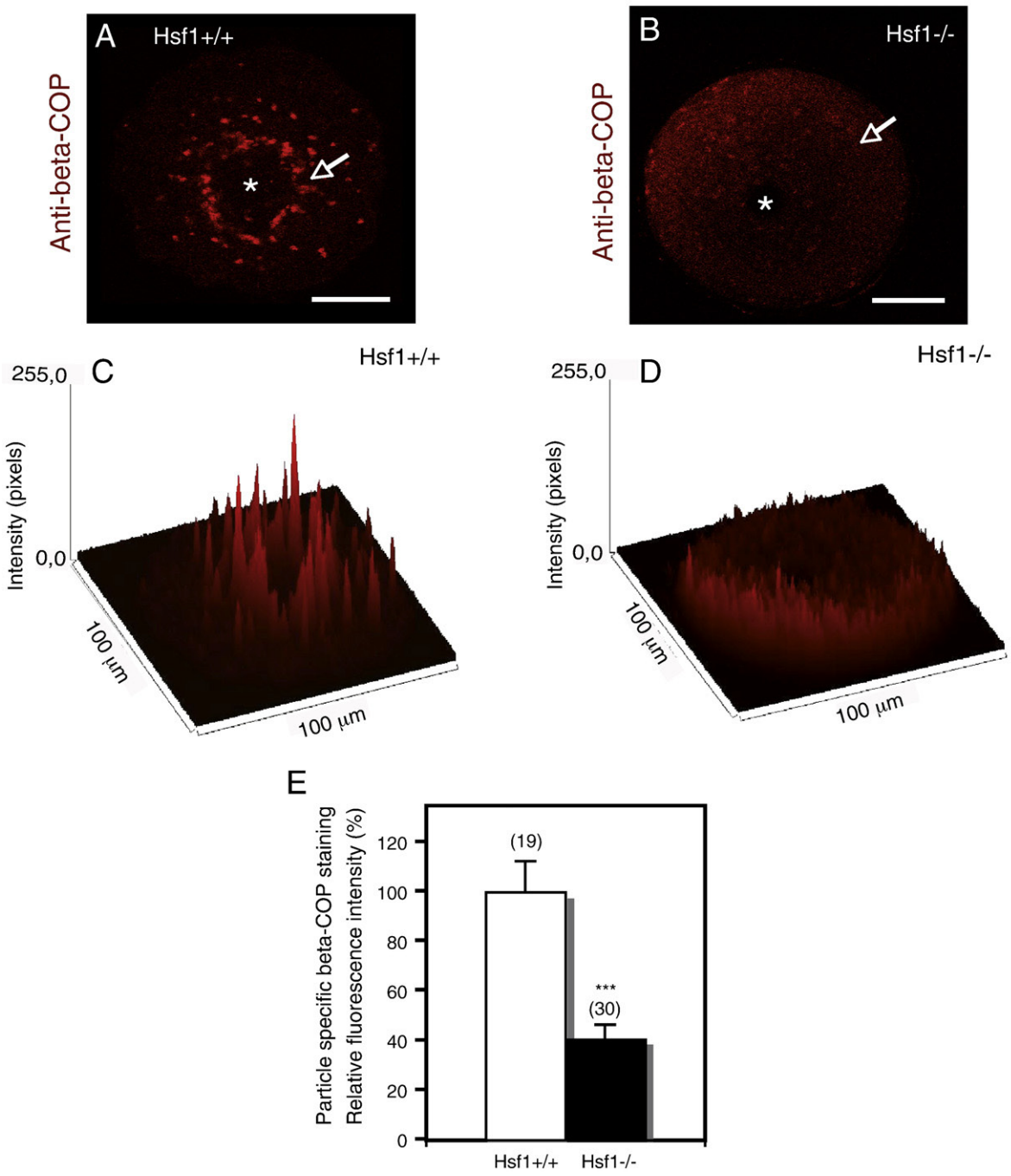

Fig. 7. Immunofluorescence for beta-COP in pre-ovulatory oocytes showing Golgi apparatus localization. (A, B) GV oocytes from WT female (A) and *Hsf1*$^{-/-}$ females were processed for immunofluorescence using antibodies against the Golgi membrane marker beta-COP and analyzed by confocal microscopy. (A) Golgi compartments appear as highly beta-COP-positive particles (arrow), enriched in proximity to the GV (asterisk) and localized throughout the ooplasm. Note the dark background, indicative of very low beta-COP cytoplasmic diffusion. (B) Mutant GV oocyte, with fewer and less strongly labelled beta-COP-positive particles (arrow). Note the higher background staining, indicative of beta-COP cytoplasmic diffusion. Scale bars represent 20 µm. (C, D) Surface plot diagram of the images in (A) and (B). The staining intensities (pixels) are plotted against the spatial X/Y coordinates. Note the wide distribution of low-intensity peaks in the mutant oocyte (D), whereas the few high-intensity peaks of beta-COP staining are characteristic of WT oocytes (C). (E) Quantification of beta-COP-specific particle staining in 19 WT ($N=3$ females) and 30 mutant GV oocytes ($N=3$ females), calculated from the total signal of particles after subtraction of the background signal; *Hsf1*$^{-/-}$ values are calculated in relation to WT values, which are normalized to 100%. Results are presented as mean percentage calculated from 3 independent experiments, and error bars correspond to SEM. Observed distribution for each phenotype in mutant group was compared with wild type group (Table S7; $p<0.001$).

severely reduced due to post-ovulation defects and second, we demonstrate that HSF1-dependent redox-balance is disturbed in mutant oocytes, resulting in cell death.

Hsf1 knock-out, a genetic model for defective redox-balance

HSF was initially known as a stress factor activated when cells were exposed to inappropriate environmental conditions, such as heat shock. However, because of HSF1 responsiveness to oxidative stress (Jacquier-Sarlin and Polla, 1996; Zhong et al., 1998), it was also suggested that physiological demands, imposed by oxidative phosphorylation and generation of ROS, require the specific intervention of HSF1 to maintain redox-homeostasis in various tissues. Since HSF1 is a transcriptional factor, special attention should be paid to its target genes, which are responsible for the multifaceted functions that are altered by *Hsf1* loss of function. We previously reported that several

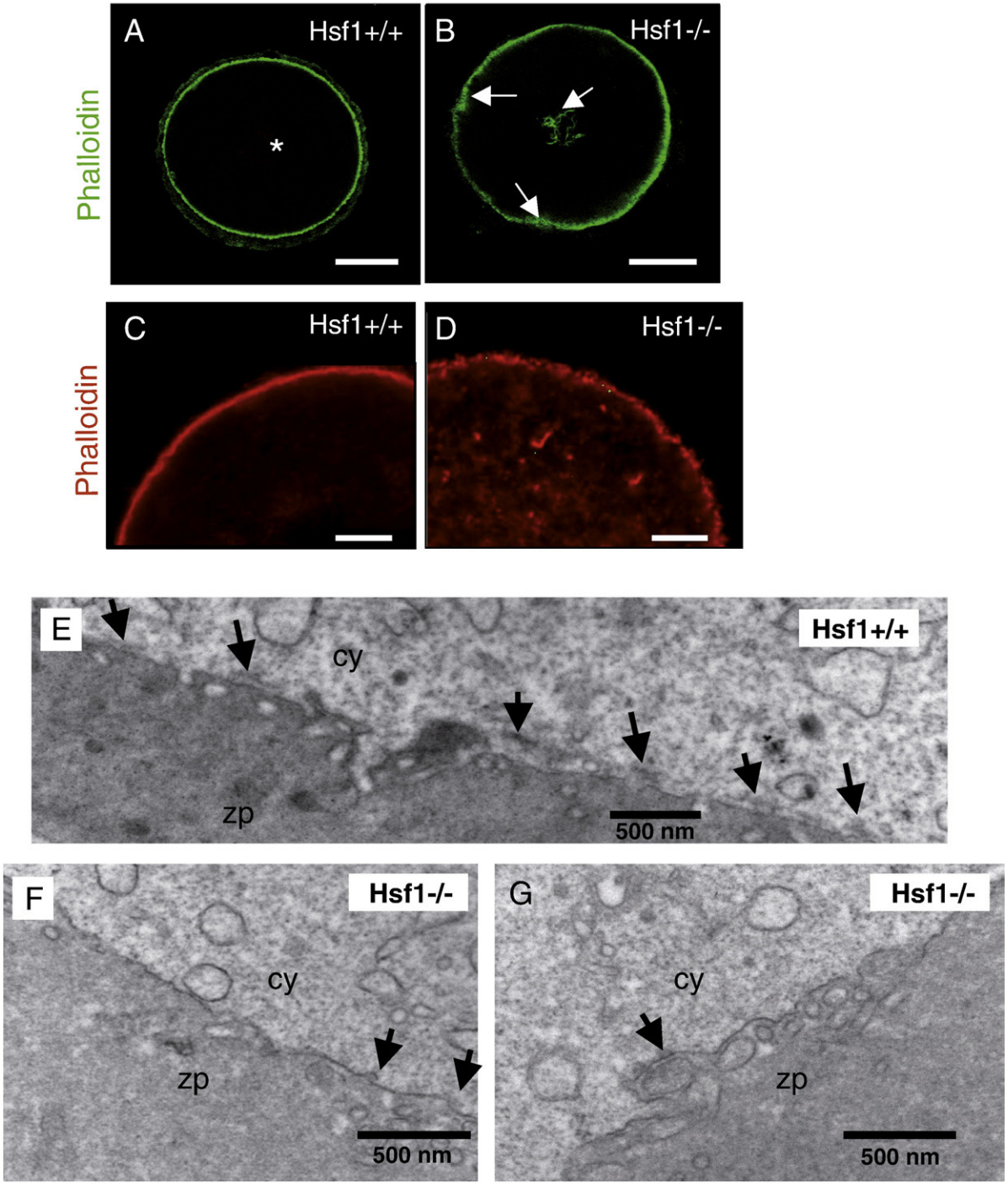

Fig. 8. Actin cytoskeleton in pre-ovulatory oocytes. (A-D) GV oocytes from WT females and *Hsf1*$^{-/-}$ females were processed for immunofluorescence using phalloidin and analyzed by confocal microscopy. (A) Image of an entire GV oocyte, showing particularly dense and concentrated phalloidin staining in the cortex underneath the membrane. Note the germinal vesicle (asterisk). (B) In the mutant GV oocyte, this cortical staining is lighter and diffuse (peripheral arrows); some F-actin is localized at the level of the GV (central arrow). (C, D) Images of phalloidin-stained cortex of WT and *Hsf1*$^{-/-}$ oocytes, at higher magnification. Note in (D) the interrupted, dotted-like staining at the cortex, but also in the cytoplasm of mutant oocytes. (E–G) Electron microscopy of pre-ovulated WT (E) and *Hsf1*$^{-/-}$ oocytes (F, G) focusing on oocyte cortex with cytoplasm (cy), plasma membrane and zona pellucida (zp). (E) WT oocyte cortex with continuous electron-dense structures (arrows) beneath the plasma membrane, indicative of a continuous actin cytoskeleton. (F, G) Mutant oocyte cortex presenting plasma membrane, basically devoid of these continuous filaments, except at some localized positions (arrows), indicative of a disorganized actin cytoskeleton. Scale bars: (A, B) 20 μm; (C, D) 10 μm; (E–G) 500 nm.

Hsp genes (Hsp25, Hsp70.1, Hsp90α, Hsp105 (Metchat et al., 2009)) and Hsc70 (Table 1 and our unpublished data)) are downregulated in *Hsf1*$^{-/-}$ oocytes. For instance, in heart and kidney, Yan and collaborators demonstrated that HSF1 deficiency coincided with a) a decreased expression of Hsps (Table 1); b) increased oxidative stress and c) ROS-induced damage to mitochondrial proteins of the mitochondrial permeability transition pore increasing mitochondrial permeability (Yan et al., 2002, 2005). These significant alterations, observed in two different *Hsf1*$^{-/-}$ tissues, did not severely modify organ morphology and function but data on mitochondrial ultrastructure were not available. In contrast, in oocytes collected from *Hsf1*$^{-/-}$ females, increased oxidative stress was accompanied by a complete loss of developmental function, as described in the present paper. Therefore, it is likely, that in the *Hsf1*$^{-/-}$ oocyte, reduced Hsps

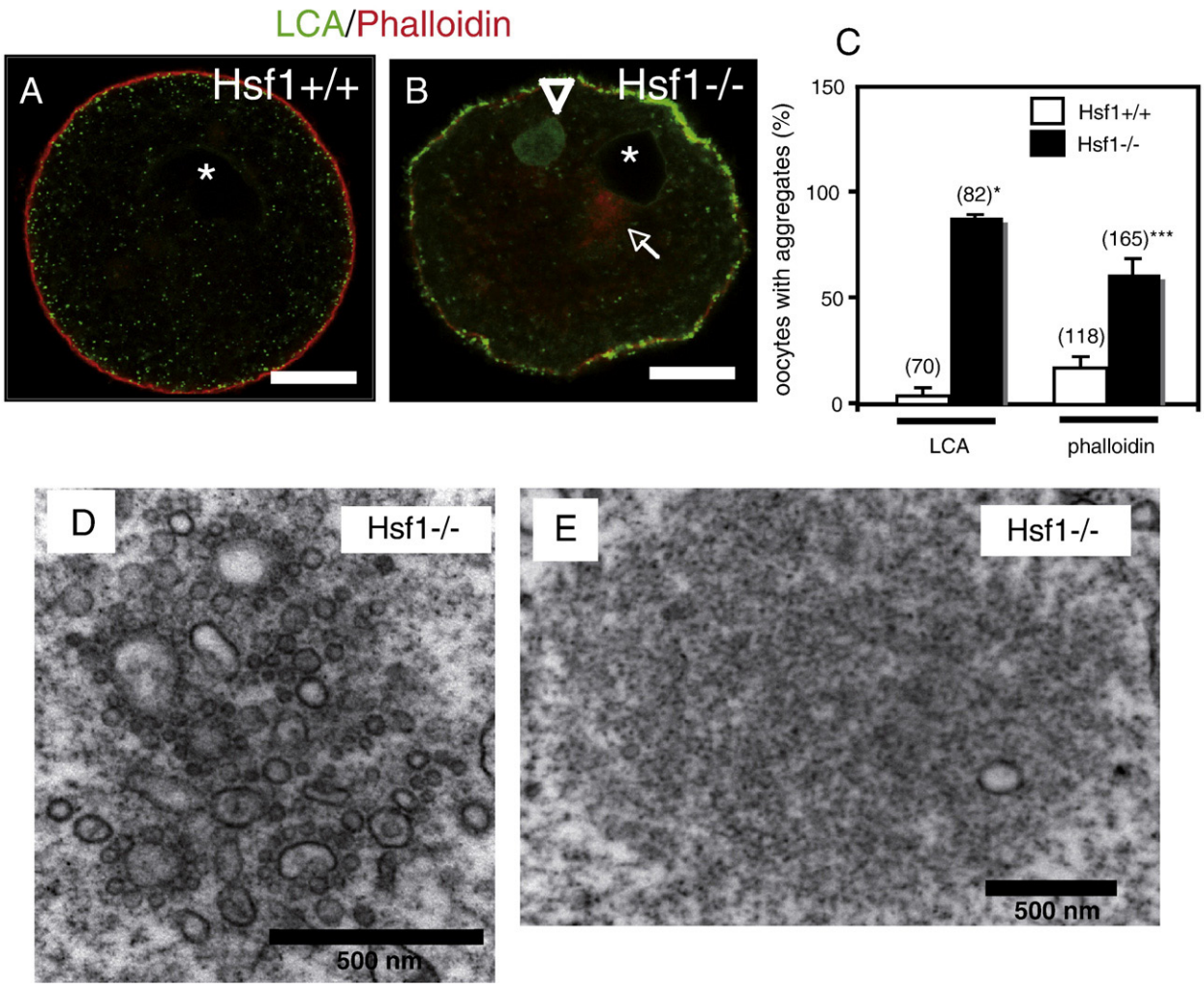

Fig. 9. Vesicular and filamentous aggregates in pre-ovulatory mutant oocytes. (A, B) Immunofluorescence of WT (A) and mutant (B) GV oocytes for cortical granules using LCA-FITC (green) and F-actin using phalloidin (red). (A) WT oocyte showing cortical granules at the membrane, colocalising with F-actin, and in the cytoplasm, but devoid of aggregates. (B) Mutant oocyte displaying one type of vesicular aggregate (green, arrowhead) and one filamentous aggregate (red, arrow) in proximity to the GV (asterisk). (C) Quantification of the proportion of WT and mutant oocytes presenting LCA- or phalloidin-positive aggregates. Results are presented as mean percentage calculated from 8 independent experiments; error bars correspond to SEM. Observed distribution for each phenotype in the mutant group was compared with the WT group (Table S8; $p<0.05$ and $p<0.001$). (D, E) Electron microscopy of mutant pre-ovulatory oocytes (ovaries). (D) Vesicular aggregates in mutant oocytes consisting of a concentration of vesicles in an electron-dense region. (E) Electron-dense area in mutant oocyte. Scale bars: (A, B) 20 μm; (D, E) 500 nm.

expression, in a similar way as for heart and kidney, may affect the redox-balance and lead to mitochondrial dysfunction because of oxidative stress-mediated damage to mitochondrial proteins, and to abnormal mitochondrial architecture due to the intimate relation between mitochondrial structure and function (Ramalho-Santos et al., 2009).

Our study using the *Hsf1*$^{-/-}$ genetic model under physiological conditions is consonant with other investigations, in which oocytes and early embryos were experimentally exposed to oxidative stress, and from which the authors concluded that oocytes and, in particular, their mitochondria, were highly sensitive to environmental perturbations (Liu et al., 1999; 2000; Dumollard et al., 2007; Somfai et al., 2007). Thus, the *Hsf1* knock-out constitutes an interesting model to study the tissue-specific impact of oxidative stress, and our work reveals that fully grown oocytes appear to be the most sensitive cells with respect to HSF1-dependent redox-homeostasis.

Mitochondria and HSF1 maternal effects

Mitochondria play a central, multifaceted maternal role in the oocyte, contributing to energy production, redox- and Ca^{2+} homeostasis, intermediate metabolite generation and storage of pro-apoptotic factors. Evidence for the central role of mitochondrial integrity in oocyte and post-fertilization development derives from studies in which mitochondrial activity was monitored before and after fertilization, as well as in the presence of pharmacological inhibitors of oxidative respiration. The results of these experiments demonstrated that mitochondrial function was also crucial for the maintenance of sperm-induced Ca^{2+} signals, as well as for the initiation and the progression of early development (Dumollard et al., 2004, 2007).

Importantly, mitochondria accumulate during oocyte growth, are only transmitted maternally and do not replicate until gastrulation so that post-ovulation, post-fertilization and cleavage development entirely relies on the inherited maternal organelles (Jansen, 2000). It has been shown that oxidative phosphorylation is maintained at a low level in oocyte mitochondria, so that only low levels of damaging ROS are generated and mitochondria are preserved (Dumollard et al., 2004). Consequently, both naturally occurring mitochondrial dysfunction (e.g., maternally aging oocytes (Tarín, 1996; Fissore et al., 2002) and oocytes of FVB strain females (Perez et al., 2007)), as well as experimentally induced mitochondrial dysfunction can result in several pre- and postovulatory phenotypes including defective meiosis, parthenogenetic activation, abnormal

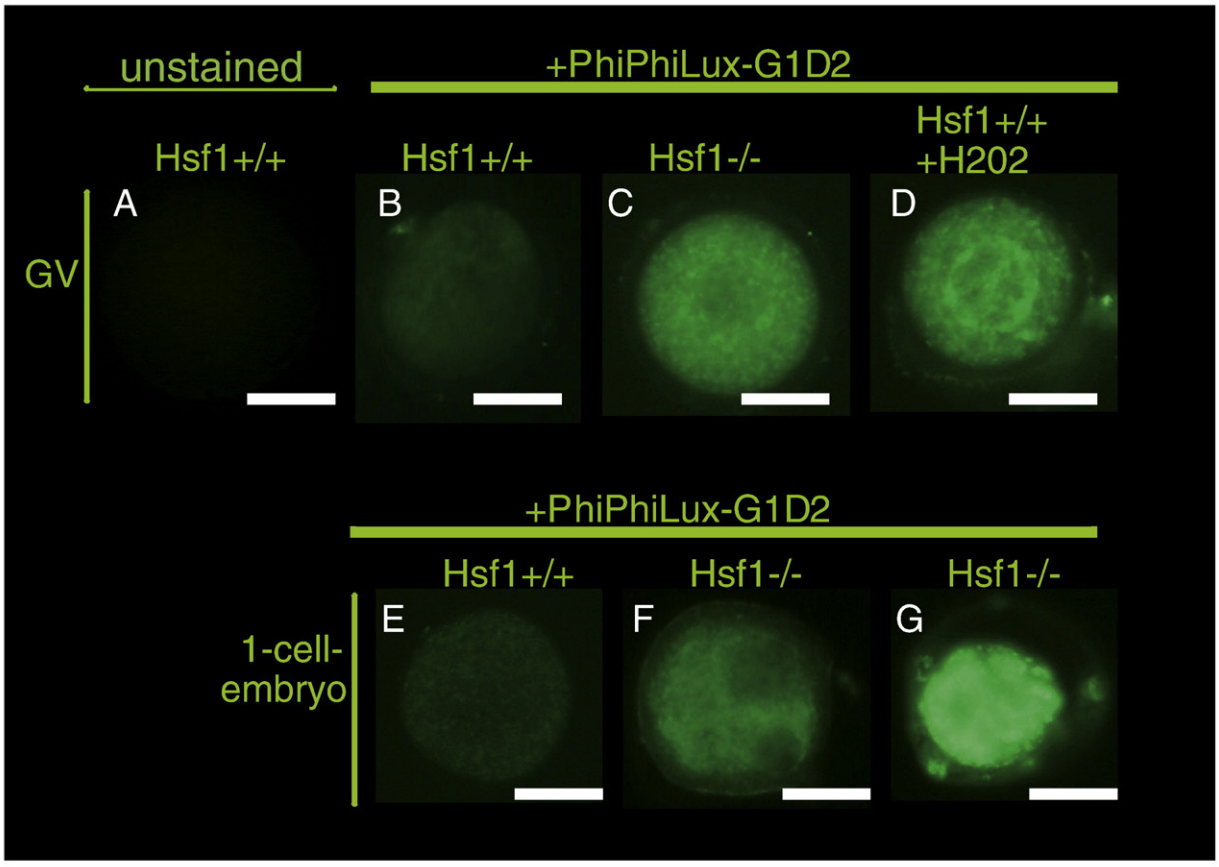

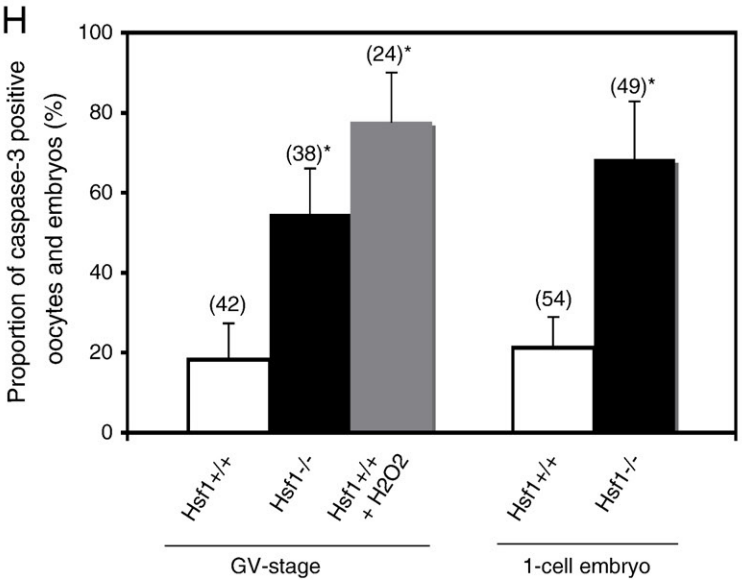

Fig. 10. Effect of lack of maternal HSF1 on the induction of apoptosis in oocytes and zygotes. (A–G) Experimental set-up: WT (A, B, D, E) and *Hsf1*$^{-/-}$ (C, F, G) GV oocytes (A–D) and 1-cell embryos (E–G) were dissected and incubated without (A) or with (B–G) the fluorogenic substrate, PhiPhiLux-G1D2 (green) of the apoptosis effector, Caspase-3, and analyzed by fluorescence microscopy ($\lambda_{ex}=488$ nm, $\lambda_{em}=520$ nm) to measure fluorescence of single oocytes and 1-cell embryos. For positive caspase-3 activation control, a set of WT GV oocytes was exposed to oxidative insult by incubation in medium containing 200 μM H_2O_2 for 1 h before analysis. (A) unstained oocyte; (B) stained WT oocyte; (C) stained *Hsf1*$^{-/-}$ oocyte; (D) stained WT oocyte after oxidant insult. Note the increased fluorescence for the oocytes in (C) *Hsf1*$^{-/-}$ and (D) WT after oxidant insult, compared with (B). (E) Stained WT zygote; (F, G) stained *Hsf1*$^{-/-}$ 1-cell embryos. Note the higher fluorescence in *Hsf1*$^{-/-}$ embryos (F) and particularly in (G) showing a degenerated oocyte/zygote, the latter type was rather rarely observed. Scale bars: (A–G) 40 μm. (H) Quantification of apoptotic WT and *Hsf1*$^{-/-}$ oocytes; WT oocytes after oxidant insult and 1-cell embryos based on fluorescence of the caspase-3 substrate, PhiPhiLux-G1D2. Results are presented as mean percentage calculated from 4 independent experiments, and error bars correspond to SEM. Observed distribution for each phenotype in the mutant group was compared with the wild-type group (Table S10; $p<0.05$).

fertilization (polyspermy), apoptosis and poor embryonal development (Thouas et al., 2004, 2005, 2006; Takeuchi et al., 2005; Dumollard et al., 2009; Van Blerkom, 2009) and atresia. In particular concerning the oocytes of the FVB strain, Perez and collaborators could demonstrate the link between abnormal mitochondrial ultrastructure, dysfunction and apoptosis (Perez et al., 2007).

In *Hsf1*$^{-/-}$ oocytes, we found higher ROS levels, indicative of increased oxidant load. In addition, mitochondrial architecture was

Table 1
Cell/tissue-specific changes in Hsp expression upon HSF1 deficiency.

Transcript and/or protein level	Hsp25	Hsp60	Hsp70.1	Hsp90α	Hsp90β	Hsp105	αB-crystallin	Hsc70[a]
Hsf1$^{-/-}$ oocytes[b]	Reduced	Not affected	Reduced	Reduced	Not affected	Reduced	N.A.	Reduced
Hsf1$^{-/-}$ kidney[c]	Reduced	Not affected	Not affected	Reduced	Not affected	N.A.	Not affected	N.A.
Hsf1$^{-/-}$ heart[d]	Reduced	Not affected	Reduced	Not affected	Not affected	N.A.	Reduced	N.A.

[a]our unpublished data; [b]Metchat et al., 2009; [c]Yan et al., 2002; [d]Yan et al., 2005.
N.A. = Not analyzed.

altered in *Hsf1*$^{-/-}$ oocytes and the level of oxidized flavoproteins (FAD^{++}) increased, further demonstrating mitochondrial dysfunction. Since mitochondria regulate redox-balance, these results reveal once more the positive feedback loop between stress and mitochondrial dysfunction, stress causing increased mitochondrial dysfunction, which, in turn, causes increased stress. As observed in somatic cells after stress (Welch and Suhan, 1985; Schwarz et al., 1998), increased stress in *Hsf1*$^{-/-}$ oocytes could further induce the alterations of the Golgi complex, cytoskeleton and in the cytoplasm that we have described here. Importantly, exocytosis of cortical granules during the zona reaction depends on the cortical actin cytoskeleton, while sperm decondensation requires a reducing environment (DiMaggio et al., 1997; Sutovsky and Schatten, 1997). So it is likely that due to increased oxidative load in *Hsf1*$^{-/-}$ oocytes, the defective cortical cytoskeleton may be responsible of the defective cortical granules exocytosis and the extra sperm attachment; while the less reduced environment may inhibit both, decondensation of extra sperm and the formation of extra pronuclei. Additional studies are needed to identify the mitochondrial process that is affected in these oocytes and to assess whether mitochondrial function is similarly affected in other cell types in *Hsf1*$^{-/-}$ animals. As mitochondria also contribute to storage of pro-apoptotic factors (Dumollard et al., 2009), any alteration of mitochondrial function could trigger the intrinsic apoptotic pathway associated with mitochondrial outer membrane permeabilization and cytochrome c release (Thouas et al., 2005; Perez et al., 2007) which ultimately leads to the production of active caspase-3. This pathway was clearly stimulated in *Hsf1*$^{-/-}$ oocytes and zygotes, which displayed a higher level of fluorescence generated by a fluorogenic substrate of caspase-3 than did WT counterparts.

Increased caspase-3 activation in *Hsf1*$^{-/-}$ oocytes, together with the ultrastructural anomalies described above, demonstrates that the mutant oocytes were committed to cell death after ovulation and fertilization. Interestingly, studies on aging mouse oocytes have demonstrated that, upon fertilization, initiation of intracellular Ca^{2+} oscillations in mouse eggs signal either activation or apoptotic death, depending on the age and the quality of the mitochondria of the eggs in which the oscillations are induced. Moreover, proteins involved in Ca^{2+} homeostasis and mediating the balance between apoptosis and survival, such as Bcl2, were shown to be implicated, associating mitochondria with this switch (Gordo et al., 2002; Takahashi et al., 2009). In conclusion, in WT oocytes, an equilibrium exists between pro- and anti-apoptotic factors that favors embryo survival, whereas in HSF1-deficient oocytes, this equilibrium is significantly compromised; even though other protective pathways may function before ovulation and fertilization, they are not sufficient at these stages to sustain further development.

Hence, HSF1 is an important member of the large set of genes whose expression governs cell death pathways and it can be proposed that, because of this integrated function, HSF1 is highly implicated in the regulation of early embryonic survival (Jurisicova and Acton, 2004).

Modeling the maternal effects of HSF1

During meiotic maturation, we recently demonstrated the important role of one of the HSF1 target genes, Hsp90α, as well as the reduced activity of the MAPK pathway when Hsp90α activity was reduced in *Hsf1*$^{-/-}$ oocytes. Interestingly, we observed that *in vivo* ovulated *Hsf1*$^{-/-}$ oocytes were frequently parthenogenetically activated, a phenomenon that is reminiscent of the phenotype observed in MAPK-deficient oocytes (e.g., *Mos* $^{-/-}$ (Hashimoto et al., 1994) or UO126-treated oocytes, (Tong et al., 2003)). Beyond the specific roles of Hsp90α interacting with its client kinases, the reduction of chaperone content in *Hsf1*$^{-/-}$ oocytes, in particular Hsp25, known to regulate the glutathione/glutathionedisulfate (GSH/GSSG) ratio is likely to be involved in the observed increased oxidant load and subsequent damage (Escobedo et al., 2004). This was previously illustrated in heart and kidney from HSF1-deficient animals (Yan et al., 2002, 2005) and also demonstrated by experiments in which HSF1 activity was stimulated. In the latter, induction of Hsp expression resulted in a protective effect against oxidative stress and cell death (Katsuki et al., 2004; Trott et al., 2008). Finally, Hsps (Hsp90; Hsp70; Hsp27) are known to neutralize pro-apoptotic factors and apoptotic effectors at several steps of the apoptotic cascade (reviewed in Beere, 2005; Xanthoudakis and Nicholson, 2000).

Taking into account our data and information from the literature, we propose a model that recapitulates the cellular roles in the oocyte that depend on maternal HSF1-mediated Hsp- gene regulation (Fig. 11).

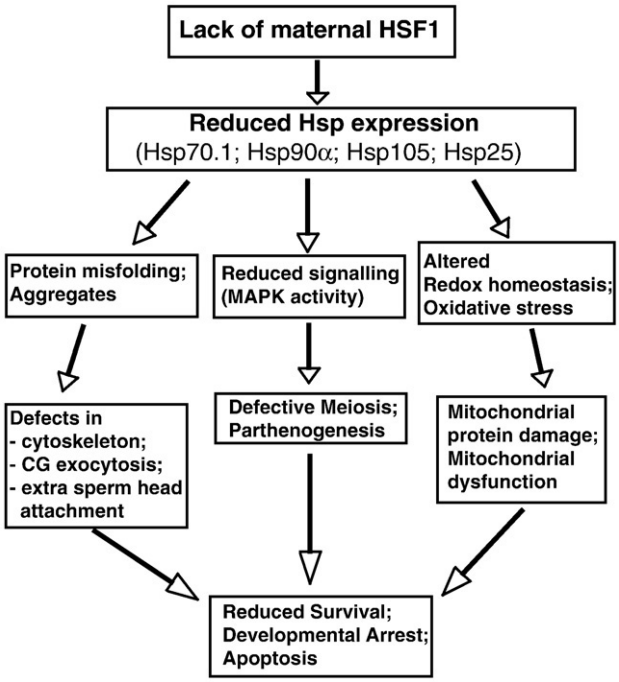

Fig. 11. Model summarizing the cellular consequences of lack of maternal HSF1 in the oocyte and embryo. Absence of maternal HSF1 leads to reduced Hsp expression (Table 1; Metchat et al., 2009), reduced signalling activity (MAPK activity), altered meiotic progression and parthenogenetic activation. Reduced Hsp expression may lead to protein misfolding and increased oxidative stress. Misfolded proteins and oxidative stress may form cytoplasmic aggregates and result in cytoskeleton disorganization; the latter may inhibit cortical granules exocytosis causing extra sperm attachment. Increased oxidative stress (increased ROS) may cause damage to mitochondrial proteins and thereby affect mitochondrial structure and function (increased FAD^{++}). Finally, dysfunctional mitochondria may compromise survival leading to apoptosis.

In summary, we propose that maternal *Hsf1* function is absolutely required to satisfy the ever increasing needs of oocytes and early embryos, in contrast to somatic cells, for defence mechanisms against oxidant load and maintenance of redox-homeostasis and mitochondrial function.

Acknowledgments

We thank Colette Charry for taking care and genotyping of *Hsf1* animals, Bruno Savelli, Brice Ronsin and Aurélie Leru for imaging, as well as Dr. Nacer Benmeradi for technical assistance with electron microscopy, (imaging facilities Toulouse RIO-imaging, IEFG-IFR109). We are indebted to the lab's of Prof. H. Alexandre and Prof. J. Carroll for their contribution to the initial steps of this work. We are grateful to our colleagues, D. Morello, L. Waltzer and A. Vincent for reading the initial version of the manuscript, as well as the members of the CBD for reagents and helpful discussions. We thank Prof. J. Smith for critically reading and improving the English version of the manuscript. This work was supported by la Fondation pour la Recherche Médicale (FRM), l'Université de Toulouse 3 (UPS), le Ministère de l'Education Nationale (AM, MRT studentship) and le Centre National pour la Recherche Scientifique (CNRS).

Appendix A. Supplementary data

Supplementary data associated with this article can be found, in the online version, at doi:10.1016/j.ydbio.2009.12.037.

References

Akerfelt, M., Trouillet, D., Mezger, V, Sistonen, L., 2007. Heat shock factors at a crossroad between stress and development. Ann. N. Y. Acad. Sci. 1113, 15–27.
Balch, W.E., Morimoto, R.I., Dillin, A., Kelly, J.W., 2008. Adapting proteostasis for disease intervention. Science 319, 916–919.
Beere, H.M., 2005. Death versus survival: functional interaction between the apoptotic and stress-inducible heat shock protein pathways. J. Clin. Invest. 115, 2633–2639.
Carabatsos, M.J., Elvin, J., Matzuk, M.M., Albertini, D.F., 1998. Characterization of oocyte and follicle development in growth differentiation factor-9-deficient mice. Dev. Biol. 204, 373–384.
Christians, E.S., Benjamin, I.J., 2006. Heat shock response: lessons from mouse knockouts. Handb. Exp. Pharmacol. 139–152.
Christians, E., Michel, E., Adenot, P., Mezger, V., Rallu, M., Morange, M., Renard, J.P., 1997. Evidence for the involvement of mouse heat shock factor 1 in the atypical expression of the HSP70.1 heat shock gene during mouse zygotic genome activation. Mol. Cell. Biol. 17, 778–788.
Christians, E., Davis, A.A., Thomas, S.D., Benjamin, I.J., 2000. Maternal effect of Hsf1 on reproductive success. Nature 407, 693–694.
Colledge, W.H., Carlton, M.B., Udy, G.B., Evans, M.J., 1994. Disruption of c-mos causes parthenogenetic development of unfertilized mouse eggs. Nature 370, 65–68.
Combelles, C.M., Gupta, S., Agarwal, A., 2009. Could oxidative stress influence the *in-vitro* maturation of oocytes? Reprod. Biomed. Online 18, 864–880.
DiMaggio Jr., A.J., Lonergan, T.A., Stewart-Savage, J., 1997. Cortical granule exocytosis in hamster eggs requires microfilaments. Mol. Reprod. Dev. 47 (3), 334–340.
Ducibella, T., 1996. The cortical reaction and development of activation competence in mammalian oocytes. Hum. Reprod. Update 2 (1), 29–42.
Dumollard, R., Marangos, P., Fitzharris, G., Swann, K., Duchen, M., Carroll, J., 2004. Sperm-triggered [Ca2+] oscillations and Ca2+ homeostasis in the mouse egg have an absolute requirement for mitochondrial ATP production. Development 131, 3057–3067.
Dumollard, R., Ward, Z., Carroll, J., Duchen, M.R., 2007. Regulation of redox metabolism in the mouse oocyte and embryo. Development 134, 455–465.
Dumollard, R., Carroll, J., Duchen, M.R., Campbell, K., Swann, K., 2009. Mitochondrial function and redox state in mammalian embryos. Semin. Cell. Dev. Biol. 20, 346–353.
Dumont, J., Million, K., Sunderland, K., Rassinier, P., Lim, H., Leader, B., Verlhac, M.H., 2007. Formin-2 is required for spindle migration and for the late steps of cytokinesis in mouse oocytes. Dev. Biol. 301, 254–265.
Escobedo, J., Pucci, A.M., Koh, T.J., 2004. HSP25 protects skeletal muscle cells against oxidative stress. Free Radic. Biol. Med. 37 (9), 1455–1462.
Eppig, J.J., Wigglesworth, K., Hirao, Y., 2000. Metaphase I arrest and spontaneous parthenogenetic activation of strain LTXBO oocytes: chimeric reaggregated ovaries establish primary lesion in oocytes. Dev. Biol. 224 (1), 60–68.
Fissore, R.A., Kurokawa, M., Knott, J., Zhang, M., Smyth, J., 2002. Mechanisms underlying oocyte activation and postovulatory ageing. Reproduction 124 (6), 745–754.
Gordo, A.C., Rodrigues, P., Kurokawa, M., Jellerette, T., Exley, G.E., Warner, C., Fissore, R., 2002. Intracellular calcium oscillations signal apoptosis rather than activation in *in vitro* aged mouse eggs. Biol. Reprod. 66 (6), 1828–1837.
Hashimoto, N., Watanabe, N., Furuta, Y., Tamemoto, H., Sagata, N., Yokoyama, M., Okazaki, K., Nagayoshi, M., Takeda, N., Ikawa, Y., et al., 1994. Parthenogenetic activation of oocytes in c-mos-deficient mice. Nature 370, 68–71.
Jacquier-Sarlin, M.R., Polla, B.S., 1996. Dual regulation of heat-shock transcription factor (HSF) activation and DNA-binding activity by H2O2: role of thioredoxin. Biochem. J. 318 (Pt 1), 187–193.
Jansen, R.P., 2000. Germline passage of mitochondria: quantitative considerations and possible embryological sequelae. Hum. Reprod. 15 (Suppl. 2), 112–128.
Jurisicova, A., Acton, B.M., 2004. Deadly decisions: the role of genes regulating programmed cell death in human preimplantation embryo development. Reproduction 128 (3), 281–291.
Katsuki, K., Fujimoto, M., Zhang, X.Y., Izu, H., Takaki, E., Tanizawa, Y., Inouye, S., Nakai, A., 2004. Feeding induces expression of heat shock proteins that reduce oxidative stress. FEBS Lett. 571, 187–191.
Kaufman, M.H., Speirs, S., 1987. The postimplantation development of spontaneous digynic triploid embryos in LT/Sv strain mice. Development 101, 383–391.
Kawamura, K., Sato, N., Fukuda, J., Kodama, H., Kumagai, J., Tanikawa, H., Shimizu, Y., Tanaka, T., 2003. Survivin acts as an antiapoptotic factor during the development of mouse preimplantation embryos. Dev. Biol. 256, 331–341.
Kregel, K.C., 2002. Heat shock proteins: modifying factors in physiological stress responses and acquired thermotolerance. J. Appl. Physiol. 92, 2177–2186.
Leader, B., Lim, H., Carabatsos, M.J., Harrington, A., Ecsedy, J., Pellman, D., Maas, R., Leder, P., 2002. Formin-2, polyploidy, hypofertility and positioning of the meiotic spindle in mouse oocytes. Nat. Cell. Biol. 4, 921–928.
Liu, L., Trimarchi, J.R., Keefe, D.L., 1999. Thiol oxidation-induced embryonic cell death in mice is prevented by the antioxidant dithiothreitol. Biol. Reprod. 61, 1162–1169.
Liu, L., Oldenbourg, R., Trimarchi, J.R., Keefe, D.L., 2000. A reliable, noninvasive technique for spindle imaging and enucleation of mammalian oocytes. Nat. Biotechnol. 18, 223–225.
Liu, H., Kim, J.M., Aoki, F., 2004. Regulation of histone H3 lysine 9 methylation in oocytes and early pre-implantation embryos. Development 131, 2269–2280.
Liu, X.Y., Mal, S.F., Miao, D.Q., Liu, D.J., Bao, S., Tan, J.H., 2005. Cortical granules behave differently in mouse oocytes matured under different conditions. Hum. Reprod. 20, 3402–3413.
Matzuk, M.M., Lamb, D.J., 2008. The biology of infertility: research advances and clinical challenges. Nat. Med. 14, 1197–1213.
McMillan, D.R., Xiao, X., Shao, L., Graves, K., Benjamin, I.J., 1998. Targeted disruption of heat shock transcription factor 1 abolishes thermotolerance and protection against heat-inducible apoptosis. J. Biol. Chem. 273, 7523–7528.
Metchat, A., Akerfelt, M., Bierkamp, C., Delsinne, V., Sistonen, L., Alexandre, H., Christians, E.S., 2009. Mammalian heat shock factor 1 is essential for oocyte meiosis and directly regulates Hsp90alpha expression. J. Biol. Chem. 284 (14), 9521–9528.
Perez, G.I., Acton, B.M., Jurisicova, A., Perkins, G.A., White, A., Brown, J., Trbovich, A.M., Kim, M.R., Fissore, R., Xu, J., Ahmady, A., D'Estaing, S.G., Li, H., Kagawa, W., Kurumizaka, H., Yokoyama, S., Okada, H., Mak, T.W., Ellisman, M.H., Casper, R.F., Tilly, J.L., 2007. Genetic variance modifies apoptosis susceptibility in mature oocytes via alterations in DNA repair capacity and mitochondrial ultrastructure. Cell Death Differ. 14, 524–533.
Pirkkala, L., Nykanen, P., Sistonen, L., 2001. Roles of the heat shock transcription factors in regulation of the heat shock response and beyond. FASEB J. 15, 1118–1131.
Ramalho-Santos, J., Varum, S., Amaral, S., Mota, P.C., Sousa, A.P., Amaral, A., 2009. Mitochondrial functionality in reproduction: from gonads and gametes to embryos and embryonic stem cells. Hum. Reprod. Update 15 (5), 553–572.
Schupbach, T., Wieschaus, E., 1989. Female sterile mutations on the second chromosome in *Drosophila melanogaster*. I. Maternal effect mutations. Genetics 121, 101–107.
Schwarz, E.R., Pollick, C., Dow, J., Patterson, M., Birnbaum, Y., Kloner, R.A., 1998. A small animal model of non-ischemic cardiomyopathy and its evaluation by transthoracic echocardiography. Cardiovasc. Res. 39 (1), 216–223.
Somfai, T., Ozawa, M., Noguchi, J., Kaneko, H., Kuriani Karja, N.W., Farhudin, M., Dinnyés, A., Nagai, T., Kikuchi, K., 2007. Developmental competence of *in vitro*-fertilized porcine oocytes after in vitro maturation and solid surface vitrification: effect of cryopreservation on oocyte antioxidative system and cell cycle stage. Cryobiology 55 (2), 115–126.
Sun, Q.Y., 2003. Cellular and molecular mechanisms leading to cortical reaction and polyspermy block in mammalian eggs. Microsc. Res. Tech. 61, 342–348.
Sutovsky, P., Schatten, G., 1997. Depletion of glutathione during bovine oocyte maturation reversibly blocks the decondensation of the male pronucleus and pronuclear apposition during fertilization. Biol. Reprod. 56 (6), 1503–1512.
Takahashi, T., Igarashi, H., Kawagoe, J., Amita, M., Hara, S., Kurachi, H., 2009. Poor embryo development in mouse oocytes aged in vitro is associated with impaired calcium homeostasis. Biol. Reprod. 80 (3), 493–502.
Takeuchi, T., Neri, Q.V., Katagiri, Y., Rosenwaks, Z., Palermo, G.D., 2005. Effect of treating induced mitochondrial damage on embryonic development and epigenesis. Biol. Reprod. 72 (3), 584–592.
Tarín, J.J., 1996. Potential effects of age-associated oxidative stress on mammalian oocytes/embryos. Mol. Hum. Reprod. 2 (10), 717–724.
Thouas, G.A., Trounson, A.O., Wolvetang, E.J., Jones, G.M., 2004. Mitochondrial dysfunction in mouse oocytes results in preimplantation embryo arrest *in vitro*. Biol. Reprod. 71 (6), 1936–1942.
Thouas, G.A., Trounson, A.O., Jones, G.M., 2005. Effect of female age on mouse oocyte developmental competence following mitochondrial injury. Biol. Reprod. 73 (2), 366–373.

Thouas, G.A., Trounson, A.O., Jones, G.M., 2006. Developmental effects of sublethal mitochondrial injury in mouse oocytes. Biol. Reprod. 74 (5), 969–977.
Tong, C., Fan, H.Y., Chen, D.Y., Song, X.F., Schatten, H., Sun, Q.Y., 2003. Effects of MEK inhibitor U0126 on meiotic progression in mouse oocytes: microtubule organization, asymmetric division and metaphase II arrest. Cell Res. 13, 375–383.
Trinklein, N.D., Murray, J.I.L., Hartman, S.J., Botstein, D., Myers, R.M., 2004. The role of heat shock transcription factor 1 in the genome-wide regulation of the mammalian heat shock response. Mol. Biol. Cell 15 (3), 1254–1261.
Trott, A., West, J.D., Klaic, L., Westerheide, S.D., Silverman, R.B., Morimoto, R.I., Morano, K.A., 2008. Activation of heat shock and antioxidant responses by the natural product celastrol: transcriptional signatures of a thiol-targeted molecule. Mol. Biol. Cell 19, 1104–1112.
Van Blerkom, J., 2009. Mitochondria in early mammalian development. Semin. Cell. Dev. Biol. 20 (3), 354–364.
Wassarman, P.M., Josefowicz, W.J., 1978. Oocyte development in the mouse: an ultrastructural comparison of oocytes isolated at various stages of growth and meiotic competence. J. Morphol. 156, 209–235.
Xanthoudakis, S., Nicholson, D.W., 2000. Heat-shock proteins as death determinants. Nat. Cell. Biol. 2, E163–165.
Welch, W.J., Suhan, J.P., 1985. Morphological study of the mammalian stress response: characterization of changes in cytoplasmic organelles, cytoskeleton, and nucleoli, and appearance of intranuclear actin filaments in rat fibroblasts after heat-shock treatment. J. Cell. Biol 101 (4), 1198–1211.
Xiao, X., Zuo, X., Davis, A.A., McMillan, D.R., Curry, B.B., Richardson, J.A., Benjamin, I.J., 1999. HSF1 is required for extra-embryonic development, postnatal growth and protection during inflammatory responses in mice. EMBO J. 18, 5943–5952.
Yan, L.J., Christians, E.S., Liu, L., Xiao, X., Sohal, R.S., Benjamin, I.J., 2002. Mouse heat shock transcription factor 1 deficiency alters cardiac redox homeostasis and increases mitochondrial oxidative damage. EMBO J. 21, 5164–5172.
Yan, L.J., Rajasekaran, N.S., Sathyanarayanan, S., Benjamin, I.J., 2005. Mouse HSF1 disruption perturbs redox state and increases mitochondrial oxidative stress in kidney. Antioxid. Redox. Signal. 7, 465–471.
Zhong, M., Orosz, A., Wu, C., 1998. Direct sensing of heat and oxidation by Drosophila heat shock transcription factor. Mol. Cell 2, 101–108.